Article

Cell Reports

ZMYND8 Co-localizes with NuRD on Target Genes and Regulates Poly(ADP-Ribose)-Dependent Recruitment of GATAD2A/NuRD to Sites of DNA Damage

Graphical Abstract

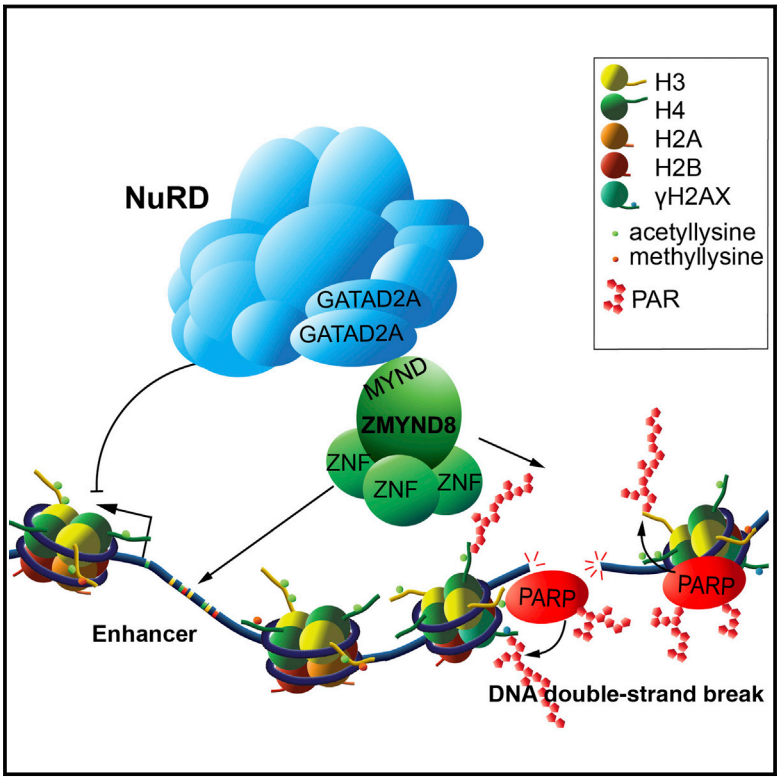

Authors

Cornelia G. Spruijt, Martijn S. Luijsterburg, Roberta Menafra, ..., Hendrik G. Stunnenberg, Haico van Attikum, Michiel Vermeulen

Correspondence

h.stunnenberg@ncmls.ru.nl (H.G.S.), h.van.attikum@lumc.nl (H.v.A.), michiel.vermeulen@science.ru.nl (M.V.)

In Brief

Spruijt et al. show that the ZMYND8 MYND domain interacts with PPPLΦ motifs in the NuRD subunit GATAD2A. Furthermore, GATAD2A and GATAD2B define mutually exclusive NuRD subcomplexes. The interaction between ZMYND8 and GATAD2A is required for poly(ADP-ribose)-dependent recruitment of NuRD to DNA double-strand breaks.

Highlights

- ZMYND8 MYND domain interacts with PPPLΦ motifs in NuRD subunit GATAD2A
- GATAD2A and GATAD2B define mutually exclusive NuRD subcomplexes
- ZMYND8 and NuRD co-localize on active (super)enhancers and promoters
- ZMYND8 recruits GATAD2A/NuRD to DNA breaks in a poly(ADP-ribose)-dependent manner

Accession Numbers

PXD003856
GSE79836

Spruijt et al., 2016, Cell Reports *17*, 783–798
October 11, 2016
http://dx.doi.org/10.1016/j.celrep.2016.09.037

Cell Reports
Article

OPEN ACCESS
CellPress

ZMYND8 Co-localizes with NuRD on Target Genes and Regulates Poly(ADP-Ribose)-Dependent Recruitment of GATAD2A/NuRD to Sites of DNA Damage

Cornelia G. Spruijt,[1,2,5] Martijn S. Luijsterburg,[3,5] Roberta Menafra,[2,6] Rik G.H. Lindeboom,[2] Pascal W.T.C. Jansen,[2] Raghu Ram Edupuganti,[2] Marijke P. Baltissen,[2] Wouter W. Wiegant,[3] Moritz C. Voelker-Albert,[1,7] Filomena Matarese,[2] Anneloes Mensinga,[1] Ina Poser,[4] Harmjan R. Vos,[1] Hendrik G. Stunnenberg,[2,*] Haico van Attikum,[3,*] and Michiel Vermeulen[2,8,*]

[1]Department of Molecular Cancer Research, University Medical Center Utrecht, 3584 CG Utrecht, the Netherlands
[2]Department of Molecular Biology, Faculty of Science, Radboud Institute for Molecular Life Sciences, Radboud University Nijmegen, 6525 GA Nijmegen, the Netherlands
[3]Department of Human Genetics, Leiden University Medical Center, 2333 ZC Leiden, the Netherlands
[4]Max Planck Institute for Molecular Cell Biology and Genetics, 01307 Dresden, Germany
[5]Co-first author
[6]Present address: École Supérieure de Physique et de Chimie Industrielles de la Ville de Paris (ESPCI ParisTech), 75231 Paris Cedex 05, France
[7]Present address: Biomedical Center, LMU, 80539 Munich, Germany
[8]Lead Contact
*Correspondence: h.stunnenberg@ncmls.ru.nl (H.G.S.), h.van.attikum@lumc.nl (H.v.A.), michiel.vermeulen@science.ru.nl (M.V.)
http://dx.doi.org/10.1016/j.celrep.2016.09.037

SUMMARY

NuRD (nucleosome remodeling and histone deacetylase) is a versatile multi-protein complex with roles in transcription regulation and the DNA damage response. Here, we show that ZMYND8 bridges NuRD to a number of putative DNA-binding zinc finger proteins. The MYND domain of ZMYND8 directly interacts with PPPLΦ motifs in the NuRD subunit GATAD2A. Both GATAD2A and GATAD2B exclusively form homodimers and define mutually exclusive NuRD subcomplexes. ZMYND8 and NuRD share a large number of genome-wide binding sites, mostly active promoters and enhancers. Depletion of ZMYND8 does not affect NuRD occupancy genome-wide and only slightly affects expression of NuRD/ZMYND8 target genes. In contrast, the MYND domain in ZMYND8 facilitates the rapid, poly(ADP-ribose)-dependent recruitment of GATAD2A/NuRD to sites of DNA damage to promote repair by homologous recombination. Thus, these results show that a specific substoichiometric interaction with a NuRD subunit paralogue provides unique functionality to distinct NuRD subcomplexes.

INTRODUCTION

The nucleosome remodeling and histone deacetylase (NuRD) complex is a highly conserved chromatin-remodeling complex that is generally associated with transcriptional repression (Allen et al., 2013). Several NuRD complex subunits are rapidly recruited to sites of DNA damage and play roles in DNA-damage-induced transcriptional repression (Chou et al., 2010; Gong et al., 2015; Larsen et al., 2010; Polo et al., 2010; Smeenk et al., 2010). The NuRD complex contains two catalytic activities: the ATP-dependent chromatin-remodeling enzymes CHD3, CHD4, and CHD5 (Allen et al., 2013; Potts et al., 2011) and the histone deacetylases HDAC1 and HDAC2. In addition to these catalytic activities, the NuRD complex contains either methyl-CpG-binding domain (MBD)2 or MBD3; GATAD2A and GATAD2B; MTA1, MTA2, and MTA3; RBBP4 and RBBP7; and CDK2AP1 (Allen et al., 2013; Hendrich and Bird, 1998; Spruijt et al., 2010, 2013). Although Smits et al. (2013) recently determined the average stoichiometry of the complex, questions remain regarding which subunits or paralogues are mutually exclusive and how many functionally distinct NuRD complexes exist.

In previous reports, we and others have identified a number of substoichiometric interactors of NuRD, including ZMYND8 and ZNF687 (Eberl et al., 2013; Kloet et al., 2014; Malovannaya et al., 2011; Smits et al., 2013). The ZNF687 protein contains ten C2H2-type zinc fingers (ZNFs), which are potential (sequence-specific) DNA-binding domains or protein-protein interaction domains. ZMYND8 has a completely different domain architecture consisting of a PHD finger, BROMO domain, and PWWP domain at its N terminus and a MYND domain located close to its C terminus. This protein is also called protein-kinase-C-binding protein (PKCBP1) or RACK7 (Ansieau and Sergeant, 2003; Fossey et al., 2000). Very recently, the PWWP domain of ZMYND8 has been linked to H3K36me2 and transcriptional regulation of retinoic-acid-induced genes during neuronal differentiation (Adhikary et al., 2016). Furthermore, the BROMO domain of ZMYND8 has been linked to transcriptional repression in response to DNA double-strand breaks (DSBs) (Gong et al., 2015).

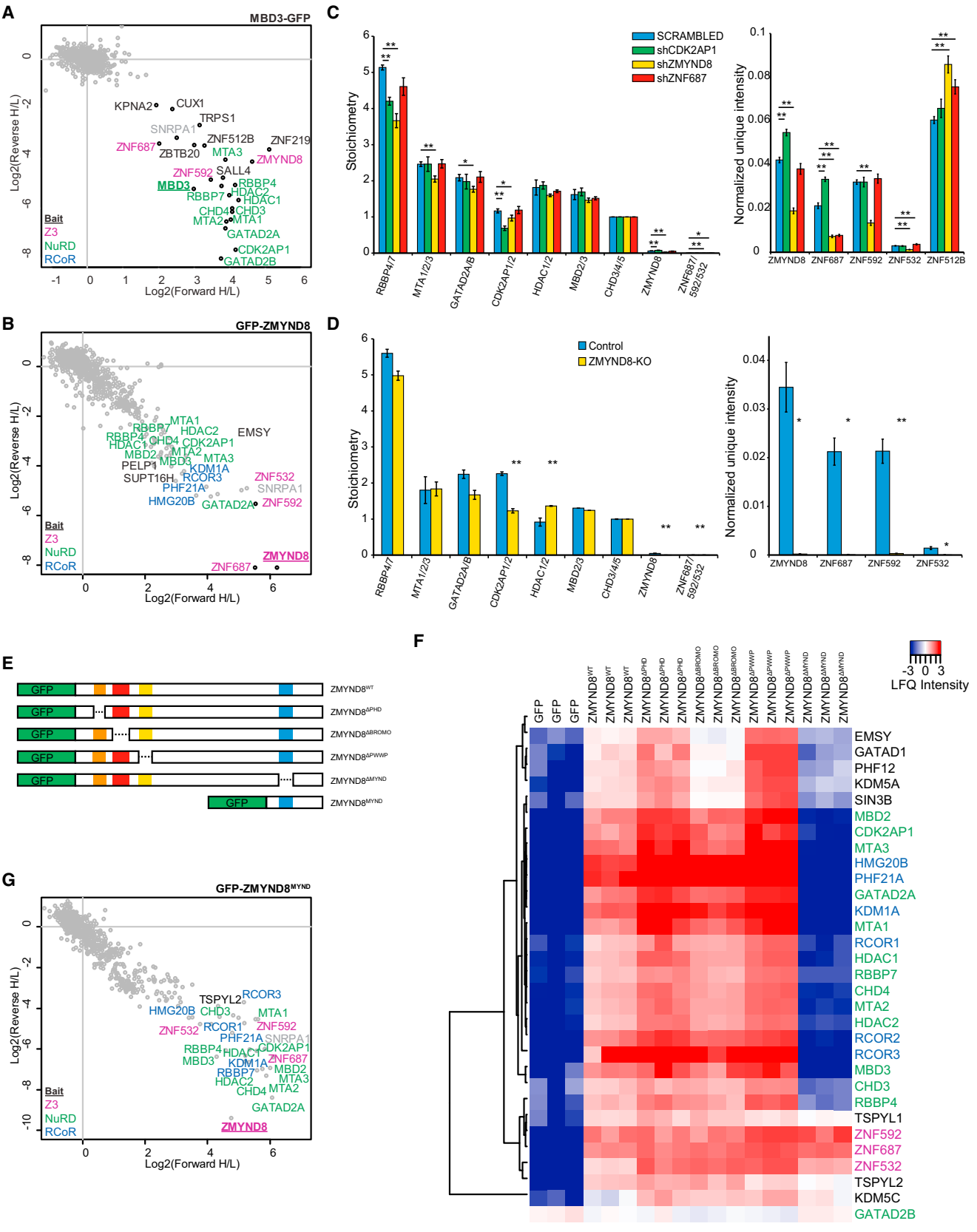

(legend on next page)

Here, we show that ZMYND8 directly interacts with the NuRD subunit GATAD2A through its conserved MYND domain and that GATAD2A and GATAD2B assemble in mutually exclusive NuRD complexes. Although the effects of ZMYND8 depletion on the recruitment to and expression of NuRD target genes are minimal, ZMYND8 plays an important role in the recruitment of GATAD2A-containing NuRD to sites of DNA damage during repair by homologous recombination. Thus, these results show that paralogue-specific substoichiometric interactions further expand the functional diversity of distinct NuRD subcomplexes.

RESULTS

ZMYND8 Connects the NuRD Complex to the Z3 Module via Its MYND Domain

Recently, ZMYND8 was identified as a novel interactor of the NuRD complex (Eberl et al., 2013; Malovannaya et al., 2011; Smits et al., 2013). To investigate the molecular nature of this interaction, we performed SILAC (stable isotope labeling with amino acid in cell culture)-based GFP affinity purifications for MBD2, MBD3, and ZMYND8 in HeLa cells (Baymaz et al., 2014). As expected, the MBD2- and MBD3-GFP purifications were significantly enriched for NuRD core subunits (Figure 1A; Figure S1A), some ZNF proteins, ZMYND8, and the known NuRD interactor SALL4. Purification of GFP-ZMYND8 resulted in the identification of the BHC complex (consisting of LSD1, RCOR1-3, PHF21A, and HMG20B), subunits of the EMSY complex (Varier et al., 2016), and the NuRD complex (Figure 1B). These results are in agreement with recent data showing that ZMYND8 and three associated ZNF proteins—ZNF532, ZNF592, and ZNF687 (Z3 module)—act as a central hub in a large transcription regulation network (Malovannaya et al., 2011).

To investigate which protein mediates the interaction between the NuRD complex and the Z3 module, we performed label-free quantification (LFQ) purifications of GFP-MBD3 from stable cell lines containing either a scrambled short hairpin RNA (shRNA) or an shRNA targeting ZMYND8, ZNF687, or CDK2AP1 (also called DOC-1) (Figures S1B and S1C) (Cox et al., 2014). We then applied the iBAQ algorithm to estimate the stoichiometry of the core NuRD subunits, ZMYND8 (3%–5%), and ZNF proteins (0%–2%) (Figure 1C, left graph) (Smits et al., 2013). Due to their sequence conservation, the three ZNF proteins share some tryptic peptides, which compromises iBAQ-based stoichiometry estimation for each individual protein. Therefore, we used the intensity of unique peptides that were identified for each ZNF protein instead of iBAQ values to estimate the relative abundance of each protein in the complex (Figure 1C, right graph). Since these values are not normalized for protein size, normalized unique intensities can only be used to compare the abundance of a single protein under different conditions. Knockdown of ZMYND8 (by ~50%) reduced the levels of the ZNF proteins interacting with MBD3 by about 50% ($p < 0.05$; Figure 1C). In contrast, knockdown (by ~60%) of ZNF687 significantly reduced the levels of ZNF687 co-purifying with NuRD, whereas the levels of the other ZNF proteins and ZMYND8 were not strongly affected. We corroborated these observations by purifying NuRD in a ZMYND8-knockout (KO) line (Figures 1D and S1D). Thus, these results reveal that ZMYND8 forms a direct link between the Z3 module and the NuRD complex.

Next, we set out to identify the domain in ZMYND8 that is required for the interaction with the NuRD complex and other interactors. ZMYND8 contains three domains that are involved in chromatin binding: a PHD finger, a BROMO domain, and a PWWP domain. In addition to these domains, ZMYND8 has a MYND (MYeloid, Nervy, and Deaf) domain, which is a well-conserved protein-protein interaction domain (Ansieau and Leutz, 2002). We generated GFP-ZMYND8 deletion constructs for all these domains (Figures 1E and S1E), which were then used in label-free-based GFP pull-down experiments. These experiments revealed that deletion of the MYND domain in ZMYND8 abolishes the interaction with the NuRD and BHC complex (Figure 1F; Figures S1F–S1I), which is in agreement with recent data from the Miller lab (Gong et al., 2015). To further substantiate these observations, we performed a SILAC-based GFP affinity purification experiment using a C-terminal fragment of ZMYND8 encompassing the MYND domain (Figure 1E). Both the NuRD and BHC complexes were specifically enriched in this pull-down experiment (Figure 1G). Altogether, these experiments show that ZMYND8 mediates the interaction between NuRD and the Z3 module and that the MYND domain in ZMYND8 is both necessary and sufficient for these interactions.

ZMYND8 Interacts with NuRD Subunit GATAD2A, which Is Mutually Exclusive with GATAD2B

Close inspection of the ZMYND8 GFP purifications (Figures 1B, 1F, and 1G) revealed that all known NuRD core subunits co-purify, with the exception of GATAD2B. The NuRD complex

Figure 1. ZMYND8 Mediates the Interaction between the Z3 Module and NuRD via Its MYND Domain

(A) SILAC-based purification of MBD3-GFP from HeLa FRT/TO cells shows all NuRD subunits and a number of substoichiometric interactors.

(B) SILAC-based purification of GFP-ZMYND8 from HeLa Kyoto. NuRD and BHC complex subunits are indicated in green and blue, respectively. ZNF proteins belonging to the Z3 module are indicated in magenta.

(C) Stoichiometry (left) and normalized unique intensity (right) graphs, respectively, of MBD3-GFP purifications from cells with shRNA-mediated scrambled, CDK2AP1, ZMYND8, or ZNF687 knockdown.

(D) Stoichiometry (left) and normalized unique intensity (right) graphs of GFP-GATAD2A purifications from Control and ZMYND8-KO cells. GFP-GATAD2A in WT cells was also used in Figures 2A and 2C.

(E) Schematic representation of the GFP-fused deletion mutants of ZMYND8.

(F) Heatmap showing the row-mean subtraction-normalized LFQ intensities of the ZMYND8 interactors (and additional NuRD subunits) in GFP purifications of ZMYND8 deletion mutants (indicated at the top). The Z3 module, NuRD, and BHC complex subunits are indicated in magenta, green, and blue, respectively.

(G) SILAC-based GFP purification of $ZMYND8^{MYND}$.

Error bars represent SD. Two-tailed Student's t test p values: *$p < 0.05$; **$p < 0.005$.

See also Figure S1 and Table S1.

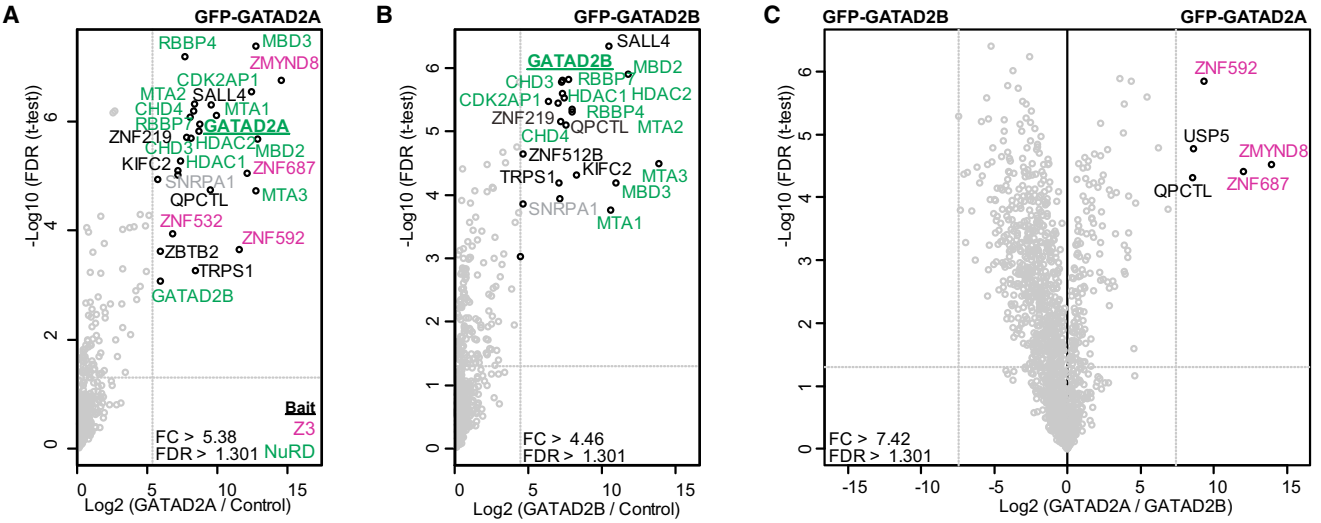

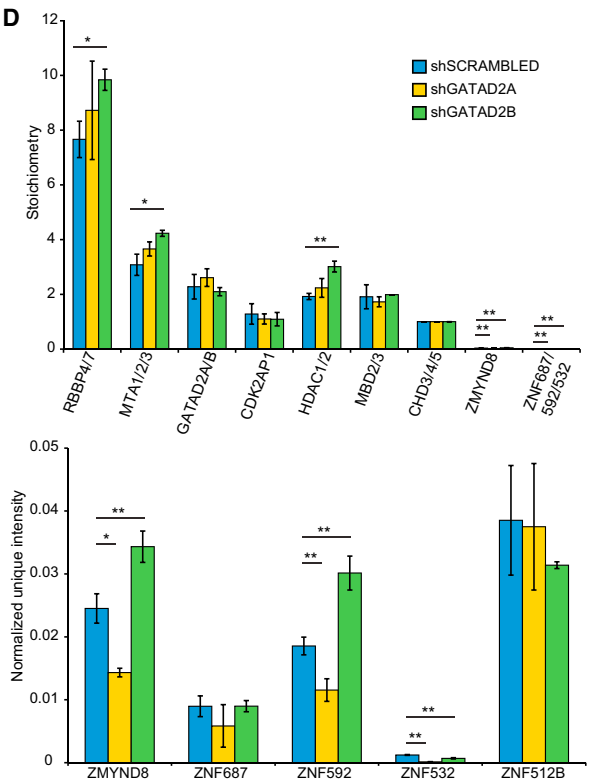

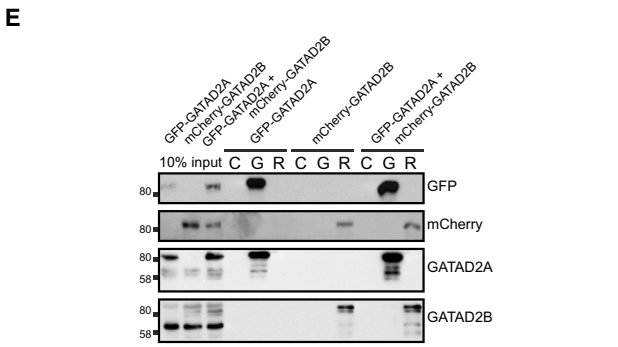

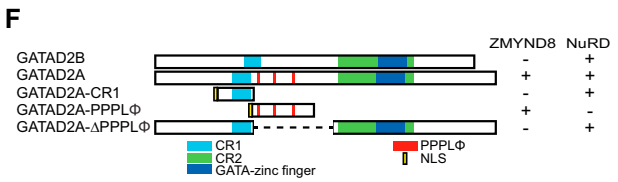

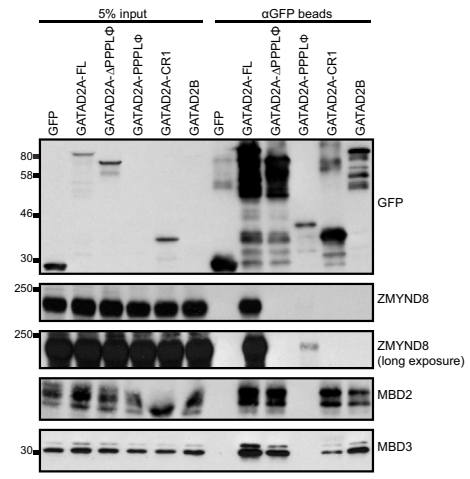

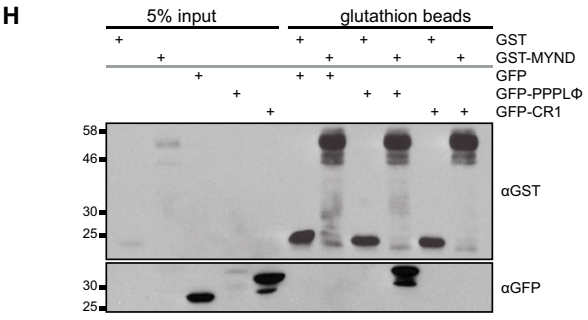

(legend on next page)

contains two GATAD2 molecules per complex (Smits et al., 2013), but whether GATAD2A and GATAD2B form heterodimers is not known. Our purifications suggest that ZMYND8 exclusively binds NuRD complexes containing GATAD2A. To further investigate this, we performed label-free GFP purifications for GATAD2A and GATAD2B (Figures 2A and 2B; Figures S2A and S2B). The GATAD2A purification resulted in enrichment of the Z3 module and all NuRD core subunits (Figure 2A). In contrast, the GATAD2B pull-down resulted in the enrichment of all NuRD subunits except GATAD2A (Figure 2B). A direct comparison of enriched proteins in the GATAD2A and GATAD2B pull-downs further confirms a specific interaction of ZMYND8 and the ZNF proteins with GATAD2A (Figures 2C and S2B). Since ZMYND8 is only enriched in GATAD2A purifications, we hypothesized that ZMYND8 interacts directly with GATAD2A. To test the importance of either GATAD2 protein for the interaction between NuRD and ZMYND8, we made use of stable GATAD2A or GATAD2B shRNA knockdown cell lines containing doxycycline-inducible expression of MBD2-GFP (Figure S2C). We purified MBD2-GFP from nuclear extracts of these cell lines. All purifications enriched for the entire NuRD complex with similar stoichiometries (Figure 2D, top; Figure S2D). The summed stoichiometry of the GATAD2 paralogues in the knockdown lines is remarkably similar to that in the control knockdown line. This implies that, in the absence of either GATAD2, the NuRD complex fully assembles using the other, available GATAD2 paralogue. We calculated the abundance of ZMYND8 and each of the ZNF proteins in the Z3 module based on unique peptides. In MBD2-GFP purifications from GATAD2B knockdown cells, ZMYND8, ZNF532, ZNF592, and ZNF687 enriched to similar, or even higher, levels compared to the control knockdown line. In contrast, lower levels of ZMYND8 and proteins of the Z3 module were present in MBD2/NuRD purifications from the GATAD2A knockdown line (Figure 2D, bottom), indicating that GATAD2A is required for the association between ZMYND8 and NuRD.

To establish whether both GATAD2A and GATAD2B form homodimers, we performed co-immunoprecipitation (coIP) experiments with GFP-GATAD2A and mCherry-GATAD2B and analyzed enriched proteins by western blot using antibodies against tagged and endogenous GATAD2A and GATAD2B (Figure 2E). Indeed, purification of GFP-GATAD2A (indicated by G) showed enrichment for endogenous GATAD2A, but not for exogenous or endogenous GATAD2B, thus providing further evidence for the formation of GATAD2A homodimers. Likewise, mCherry-GATAD2B purification (indicated by R) exclusively enriched for endogenous GATAD2B but failed to enrich for endogenous or exogenous GATAD2A.

Altogether, these data revealed that GATAD2A and GATAD2B define mutually exclusive NuRD complexes, similarly to what we have previously shown for MBD2 and MBD3 (Le Guezennec et al., 2006). Furthermore, only GATAD2A-containing NuRD complexes interact with the ZMYND8/Z3 module.

GATAD2A Has Conserved MYND Interaction Motifs

ZMYND8 exclusively interacts with GATAD2A/NuRD, which suggests that ZMYND8 directly binds to a motif present in GATAD2A that is lacking in GATAD2B. MYND domains are described to recognize different proline-rich motifs, like PxLxP or PPPLΦ (Ansieau and Leutz, 2002; Kateb et al., 2013; Liu et al., 2007). Vertebrate GATAD2A contains three consensus PPPLΦ motifs, while GATAD2B lacks these motifs (Figures 2F and S2E). To test whether these motifs are required for the direct interaction with ZMYND8, we generated a PPPLΦ-deletion mutant of GATAD2A (GATAD2A$^{\Delta PPPL\Phi}$). Furthermore, we generated a GFP-fusion protein containing the PPPLΦ motifs fused to a nuclear localization sequence (NLS) (GATAD2A$^{PPPL\Phi}$). As a control, we included GATAD2A^{CR1}, which entails the conserved region that interacts with methyl-binding domain (MBD) proteins (Gnanapragasam et al., 2011) (Figure 2F). All of these constructs show a nuclear localization (Figure S2F). We transiently transfected HEK293T cells with these constructs and prepared nuclear extracts. Western blot analyses of GFP purifications from these extracts revealed that wild-type GATAD2A binds ZMYND8, while GATAD2B or GATAD2A$^{\Delta PPPL\Phi}$ failed to do so (Figure 2G). In contrast, all proteins, except GFP-GATAD2A$^{PPPL\Phi}$, interact with the NuRD subunits MBD2 and MBD3. Although the expression level of GFP-GATAD2A$^{PPPL\Phi}$ was low, a specific interaction with ZMYND8 is visible upon a longer exposure of the blot. Similar results were obtained in SILAC-based GFP-affinity purifications (Figure S2G).

To further confirm that the MYND domain of ZMYND8 directly interacts with the PPPLΦ motifs in GATAD2A, we expressed GST-ZMYND8^{MYND} in *E. coli* and purified the protein using glutathione beads. Then, we incubated the bead-coupled protein with nuclear extract containing GFP, GFP-GATAD2A^{CR1}, or GFP-GATAD2A$^{PPPL\Phi}$. Only the combination of GST-ZMYND8^{MYND} with GFP-GATAD2A$^{PPPL\Phi}$ resulted in an interaction (Figure 2H). Since GFP-GATAD2A$^{PPPL\Phi}$ does not interact with any other NuRD subunit (Figures 2G and S2G), this is a direct interaction.

Figure 2. ZMYND8 Interacts Only with the GATAD2A/NuRD Complex, which Is Mutually Exclusive with GATAD2B-Containing NuRD

(A and B) LFQ-based GFP purification of GATAD2A and GATAD2B, respectively. The Z3 module, NuRD, and BHC complex subunits are indicated in magenta, green, and blue, respectively.

(C) Direct comparison of the GATAD2A and GATAD2B purifications.

(D) Stoichiometry determination for NuRD subunits based on LFQ GFP purifications from HeLa cells expressing MBD2-GFP and either a GATAD2A or GATAD2B shRNA. As a control, purifications were performed using a scrambled shRNA cell line. Bottom graph shows the normalized unique intensities of each of the ZNF proteins in the MBD2 purifications. Error bars indicate SD. Two-tailed Student's t test p values: *$p < 0.05$; **$p < 0.005$.

(E) Co-immunoprecipitation of GFP-GATAD2A and mCherry-GATAD2B analyzed by western blot. GFP, red fluorescent protein (RFP), or control purifications are indicated by G, R, or C, respectively.

(F) Schematic representation of the different GATAD2A and B mutants used for the interaction study. An alignment of the PPPLΦ stretch is shown in Figure S2E.

(G) GFP purifications of GATAD2B and different mutants of GATAD2A analyzed by western blot.

(H) Purified GST-ZMYND8^{MYND} was used to fish for the indicated GFP-fusion proteins. Interactions were analyzed by western blot.

See also Figure S2 and Table S1.

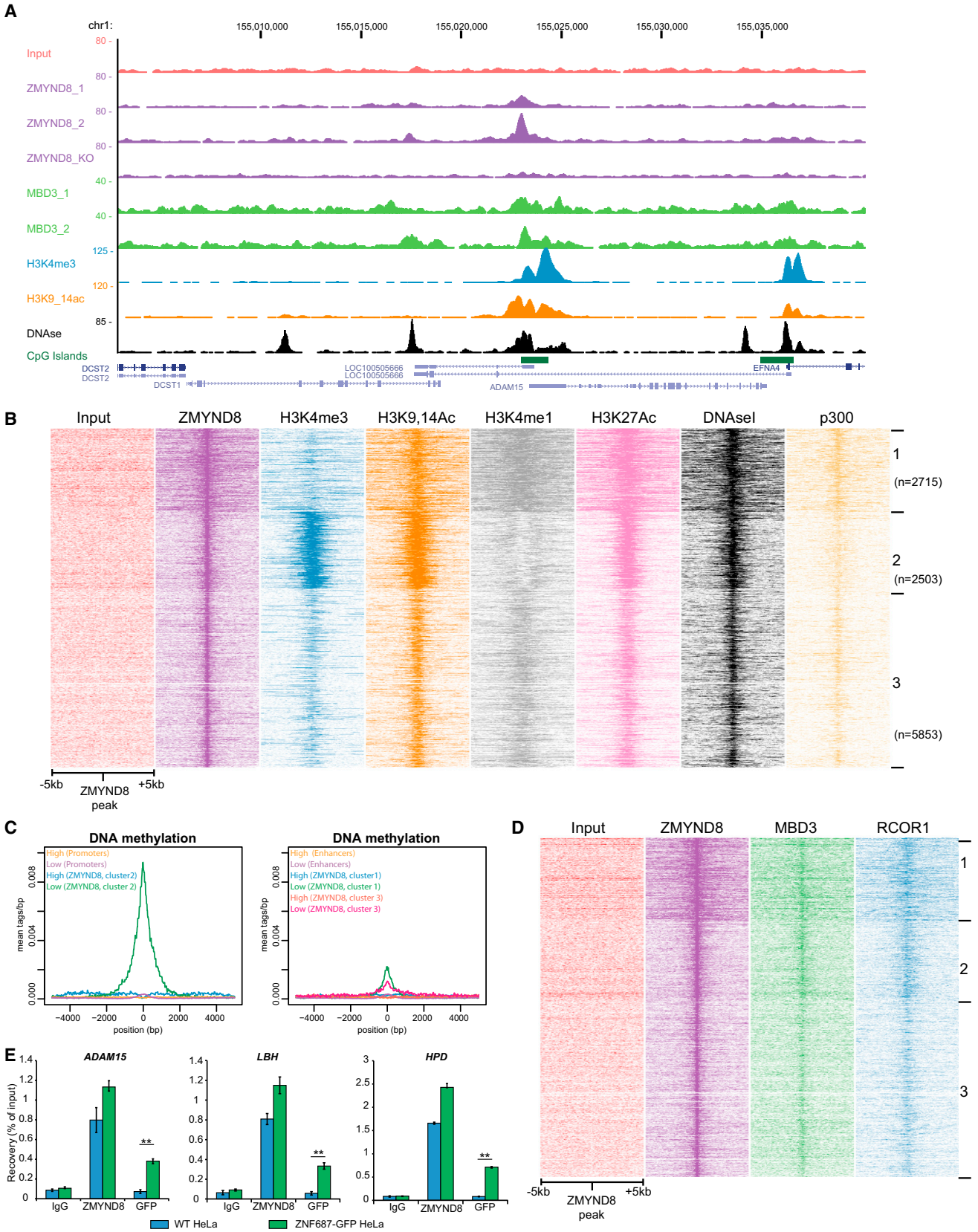

(legend on next page)

In conclusion, the MYND domain of ZMYND8 directly interacts with PPPLΦ motifs in GATAD2A.

ZMYND8 and MBD3 Occupy Active Promoters and Enhancers Genome-wide

To investigate genome-wide binding sites of ZMYND8 and MBD3, we performed chromatin immunoprecipitation sequencing (ChIP-seq) (Figure 3A). Endogenous ZMYND8 ChIP-seq resulted in ~11,000 peaks. These overlap very well with anti-GFP ChIP-seq targeting ZMYND8-GFP (Figure S3A). Furthermore, ChIP-seq for ZMYND8 in ZMYND8-KO cells confirmed that the endogenous ZMYND8 antibody is specific (Figures S3A and S3B). The number of ZMYND8 peaks detected in HeLa cells is lower compared to MCF7 cells, a breast cancer cell line that overexpresses ZMYND8 (Shen et al., 2016).

Based on co-localization with histone marks, the ZMYND8 peaks can be divided into three clusters, one of which mainly contains promoters (Figure 3B). RNA sequencing reveals that most of these promoters are actively transcribed (Figure S3C) and are marked by H3K4me3 and by H3K9, K14, and K27 acetylation (Figure S3D). The two other clusters mainly comprise (super)enhancers (marked by H3K4me1, H3K27Ac, DNase1, and lack of H3K4me3) (Figures 3B and S3D). Strikingly, ZMYND8-bound loci are depleted of DNA methylation (Figure 3C).

Both at promoters and enhancers, ZMYND8 shows a good overlap with MBD3 and RCOR1 (Figure 3D). A GFP-tagged version of ZNF687 also occupies ZMYND8 target genes, as determined by ChIP-qPCR (Figure 3E). Given the presence of many putative DNA-binding ZNFs in the Z3 module, we hypothesized that this module may serve to recruit the NuRD complex to at least a subset of its genome-wide binding sites. To address this hypothesis, we used a ZMYND8-KO cell line along with a ZMYND8-KO rescue cell line allowing doxycycline-inducible expression of GFP-ZMYND8^{WT} (Figure 4A). ChIP-qPCR revealed that GFP-ZMYND8^{WT} occupied the same binding sites compared to endogenous ZMYND8, demonstrating the functionality of the fusion protein (Figure 4B). The occupancy of endogenous NuRD subunits GATAD2A, MBD3, and CHD4 on target genes was neither significantly reduced in the ZMYND8-KO cells nor increased in the rescue cells (Figures 4B and S3E). A bandplot visualization of the average ZMYND8 and MBD3 occupancy of ZMYND8 target sites in control and ZMYND8-KO cells, as determined by ChIP-seq, reveals that while ZMYND8 is drastically reduced, MBD3 occupancy is not affected (Figures S3F and S3G). In addition, both GFP-GATAD2A and GFP-GATAD2B occupy ZMYND8 target genes (Figure S3H). Using qRT-PCR, we found no difference in the expression of ZMYND8 target genes in ZMYND8-KO versus control or rescue cells (Figure 4C). Finally, to investigate the global effects of knocking out ZMYND8 on transcription, we performed RNA sequencing (RNA-seq) on control, ZMYND8-KO, and GFP-ZMYND8^{WT} rescue cells. Interestingly, we observed significant upregulation of genes that have ZMYND8 binding at their enhancers and, especially, that super-enhancers show induced expression (Figure 4D). These observations are consistent with a recent report (Shen et al., 2016).

In conclusion, although ZMYND8 and NuRD share a large number of genome-wide binding sites, the ZMYND8/Z3 module does not serve to recruit NuRD to non-methylated target sites in the genome, at least not in steady-state asynchronous cells. Furthermore, genetic deletion of ZMYND8 has only mild effects on gene expression of its target genes.

ZMYND8 Recruits GATAD2A/NuRD to Sites of DNA Damage

Since we did not observe a clear role for ZMYND8 in recruiting NuRD to its target genes in steady-state asynchronous cells, we focused on a more dynamic system. Earlier work from us and others revealed that the NuRD complex accumulates at sites of DNA DSBs (Larsen et al., 2010; Polo et al., 2010; Smeenk et al., 2010) and that this process requires the recruitment of ZMYND8 (Gong et al., 2015). Since ZMYND8 exclusively interacts with the GATAD2A-containing NuRD complex, we tested whether ZMYND8 and GATAD2A are recruited to DSBs. Endogenous ZMYND8, as well as endogenous and GFP-tagged GATAD2A, was rapidly (<5 min) recruited to sites of laser-induced DSBs that were marked by phosphorylated H2AX (γH2AX) (Figure 5A; Figure S4A). Knockdown of GATAD2A or genetic deletion of ZMYND8 resulted in the loss of signal in laser tracks, demonstrating the specificity of the used antibodies (Figures 5A and S4B). To address whether ZMYND8 is involved in GATAD2A/B recruitment, we made use of our ZMYND8-KO cells (Figure 4A). Recruitment of GATAD2A to laser-induced DSBs was significantly reduced in ZMYND8-KO cells compared to control cells (Figures 5B and 5C). To monitor GATAD2B recruitment, we induced expression of GFP-GATAD2B in both ZMYND8-KO and control cells. We could detect rapid recruitment of GFP-GATAD2B to laser-induced DSBs (Figure 5D). However, in contrast to GATAD2A, recruitment of GFP-GATAD2B was not affected by the loss of ZMYND8 (Figures 5D and 5E), while DSB levels, as measured by γH2AX formation, were comparable in ZMYND8-KO and control cells. Next, we tested whether the ZMYND8-GATAD2A interaction is required for recruitment of the NuRD complex to DSBs. To this end, we used our inducible MBD2-GFP cell lines with stable shRNA-mediated knockdown of either GATAD2A or GATAD2B

Figure 3. ZMYND8 and MBD3 Co-occupy Active Promoters and Enhancers

(A) UCSC (University of California, Santa Cruz) browser screenshot showing co-localization of ZMYND8 and MBD3 on the *ADAM15* promoter, which is marked by H3K4me3 and H3K9,14Ac. Note that the signal for ZMYND8 is strongly reduced in ZMYND8 knockout cells (ZMYND8_KO).

(B) Heatmap centered on ZMYND8 peaks ± 5 kb. Cluster 2 contains mostly promoters, whereas clusters 1 and 3 consist of enhancers.

(C) DNA methylation analysis for ZMYND8 peaks or random genomic regions, divided into promoters and enhancers.

(D) Heatmap showing the genome-wide overlap between ZMYND8 and its interactors MBD3 and RCOR1.

(E) ChIP-qPCR analysis of GFP-ZNF687 ChIP on ZMYND8 target genes. WT, wild-type. Error bars indicate SD. Two-tailed Student's t test p values: *$p < 0.05$; **$p < 0.005$.

See also Figure S3 and Table S2.

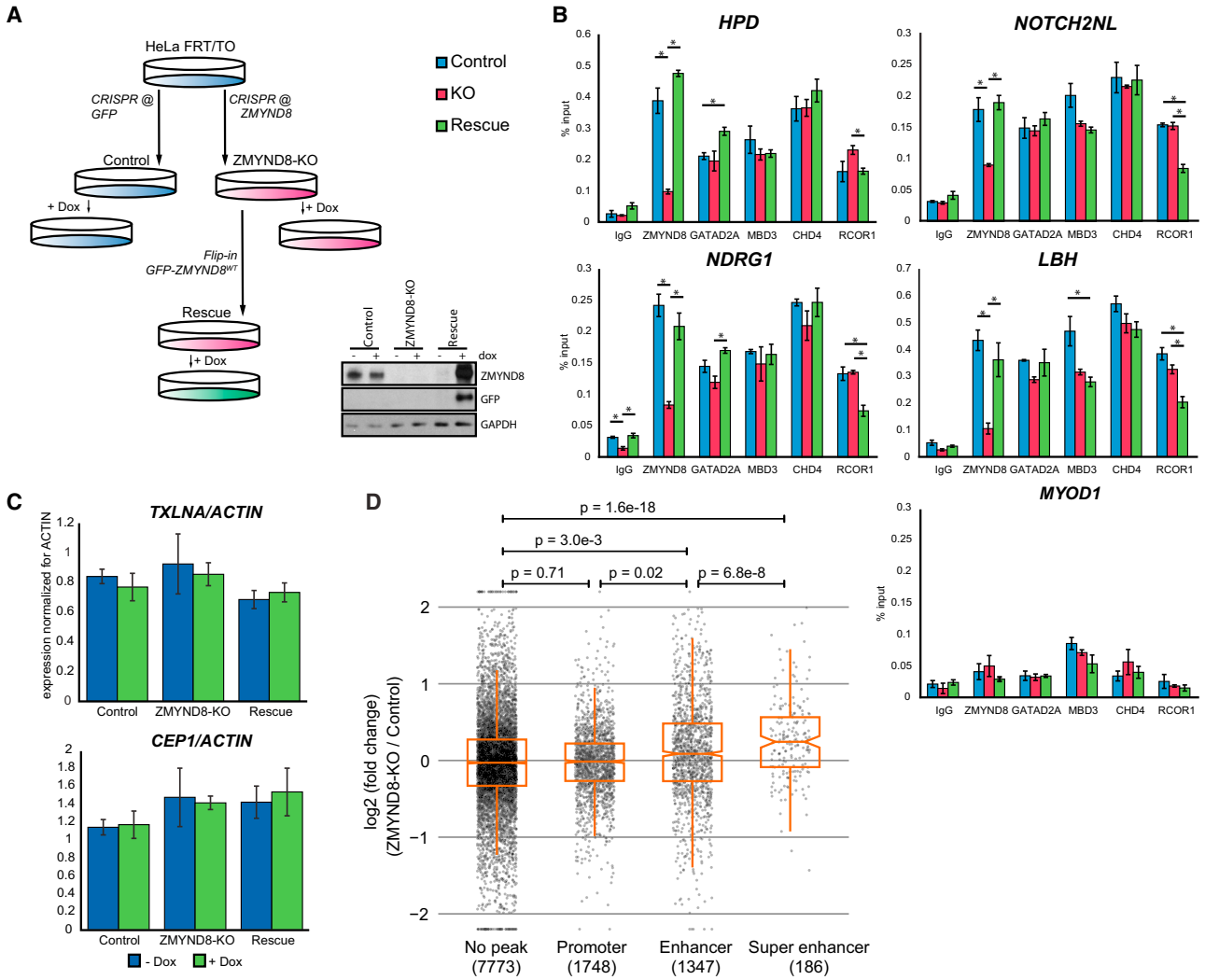

Figure 4. ZMYND8 Depletion Does Not Affect NuRD Recruitment and Only Mildly Affects Transcriptional Output of Target Genes

(A) Schematic representation of the cell lines used for the ChIPs in (B). All three cell lines were doxycycline (Dox) treated to correct for any Dox-induced artifacts.

(B) Endogenous ChIPs for ZMYND8, GATAD2A, MBD3, CHD4, and RCOR1 in control, ZMYND8-KO, and rescue cell lines.

(C) qRT-PCR analysis of ZMYND8 target genes.

(D) Expression analysis of genes with a ZMYND8 peak on their promoter or nearby enhancer. The y axis shows fold change in ZMYND8-KO over control cells. The p values were determined using a two-tailed Student's t test. Error bars in (B and C) indicate SD. Two-tailed Student's t test p values: *p < 0.05.

See also Figure S3 and Table S2.

(Figure S2C). The rapid recruitment of MBD2-GFP was significantly reduced by knockdown of GATAD2A but was unaffected by depletion of GATAD2B (Figures 5F and 5G). Importantly, DSB induction, as monitored by γH2AX, was comparable in these cells. Assessment of the MBD2-GFP recruitment in the ZMYND8-KO cells confirmed our hypothesis that MBD2 is, at least partially, recruited via the ZMYND8-GATAD2A axis (Figures 5H and 5I). Finally, we sought to address whether the ZNF proteins are involved in the DNA damage response. Local irradiation, indeed, revealed that ZNF687-GFP is rapidly recruited to laser-induced DSBs (Figure 5J). Furthermore, siRNA-mediated knockdown of ZNF687 impaired the recruitment of GFP-CHD4 to DSBs (Figures 5K and 5L). These findings highlight a sequential recruitment model for the MBD2/NuRD complex, which specifically depends on the ZMYND8/ZNF-GATAD2A axis.

The MYND Domain in ZMYND8 Regulates Its Recruitment to Sites of DNA Damage

Previous studies have revealed an important role of poly(ADP-ribose) (PAR) in the accumulation of CHD4 (Chou et al., 2010; Luijsterburg et al., 2012; Polo et al., 2010) and MBD2 (Sun et al., 2016). Although the recruitment of both these proteins is stimulated by ZMYND8 (Figure 5) (Gong et al., 2015), ZMYND8 itself was reported to be recruited to sites of DNA damage through histone acetylation (Gong et al., 2015). To further investigate these findings, we performed functional rescue experiments in our ZMYND8-KO cells. In contrast to control cells, we

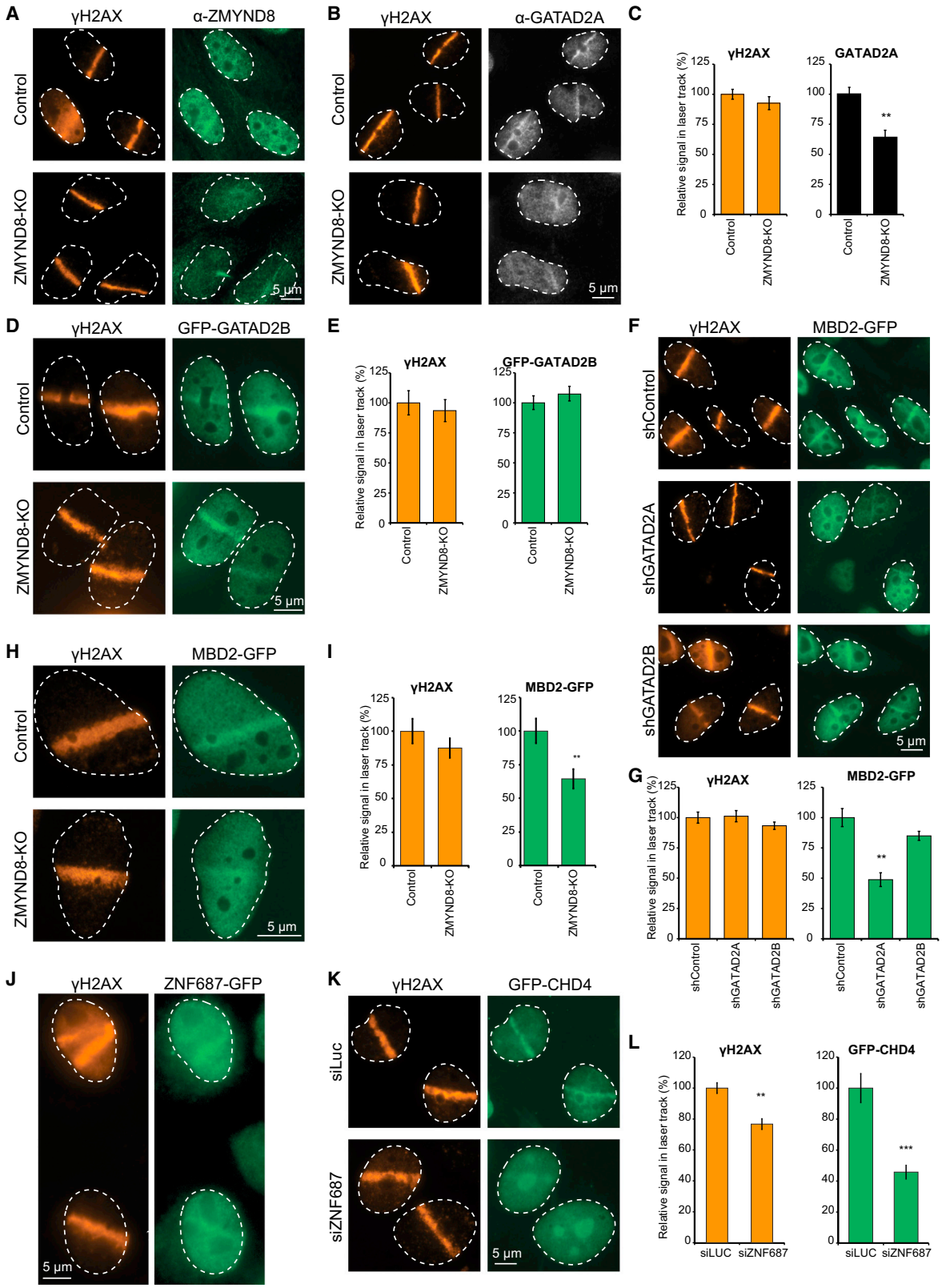

(legend on next page)

found that ZMYND8-KO cells failed to recruit endogenous CHD4 to sites of DNA damage (Figures 6A and 6B). Re-expression of ZMYND8^{WT} and ZMYND8$^{\Delta BROMO}$ fully rescued CHD4 recruitment, while ZMYND8$^{\Delta MYND}$ failed to do so (Figures 6A and 6B). Analysis of the GFP-ZMYND8 mutants also showed that recruitment of ZMYND8 to sites of DNA damage critically depends on its MYND domain (Figures 6A and 6B). These findings show that ZMYND8 recruitment itself, as well as its ability to interact with and recruit the NuRD complex, is fully dependent on its MYND domain, which is in line with our mass spectrometry (MS) data (Figure 1F). To test whether the association of ZMYND8 with the NuRD complex is further induced by DNA damage, we performed LFQ GFP purifications of MBD3 and ZMYND8 in the absence and presence of the DSB-inducing agent phleomycin. This revealed that the stoichiometry of the ZMYND8/NuRD interaction does not change upon induction of DNA damage ($p < 0.01$; Figures S5C and S5D).

Contrary to our findings, a previous study from the Miller lab reported that ZMYND8 recruitment is mediated through histone acetylation and involves its BROMO domain (Gong et al., 2015). Based on these results, we first confirmed whether our ZMYND8$^{\Delta BROMO}$ is defective in binding histone acetylation. Indeed, in vitro binding assays confirmed that our ZMYND8$^{\Delta BROMO}$ mutant fails to bind acetylated histone tails, while endogenous and GFP-ZMYND8^{WT} were proficient in doing so (Figures 6C and 6D). In an attempt to resolve this discrepancy, we transiently expressed the ZMYND8$^{\Delta BROMO}$ mutant from the Miller lab and could, indeed, confirm that this protein does not accumulate at sites of DNA damage (Gong et al., 2015) (Figure S4E). Although we did note that this mutant tends to mislocalize in the cytoplasm when expressed at higher levels, we could still detect an interaction with other NuRD subunits in pull-down experiments from nuclear extracts, suggesting at least partial functionality of the mutant. However, the human *ZMYND8* gene encodes at least 20 protein-coding transcripts, many of which produce large proteins containing all the functional ZMYND8 domains. We used a different isoform of ZMYND8 (isoform 17, 1,054 amino acids [aa]; ENST00000458360) compared to the one used by Miller (isoform 1, 1,186 aa; ENST00000396281). The discrepancy in the BROMO-dependent recruitment of ZMYND8 observed in the two studies may be explained by the use of different ZMYND8 isoforms.

Considering the previously reported involvement of PAR chains in NuRD subunit recruitment, we asked whether ZMYND8 recruitment is PAR dependent. This could reconcile our results with previous studies and possibly explain how both PAR and ZMYND8 could stimulate the recruitment of CHD4 and MBD2 (Chou et al., 2010; Luijsterburg et al., 2012; Polo et al., 2010; Sun et al., 2016). Local irradiation experiments revealed that the recruitment of GFP-ZMYND8^{WT} was completely abolished by the treatment of cells with poly(ADP-ribose) polymerase (PARP) inhibitor KU-0058948. Control experiments confirmed the complete loss of PAR chain formation under these conditions (Figures 7A and 7B). Our analysis clearly indicates that the ZMYND8 isoform 17 is functional and able to restore CHD4 recruitment to sites of DNA damage and does not require BROMO-mediated binding to acetylated histones for its recruitment to sites of DNA damage. Instead, we show that recruitment of this ZMYND8 variant fully depends on the MYND domain and requires the formation of DNA damage-induced PAR.

NuRD Subunits Regulate DSB Repair by Homologous Recombination

To address whether NuRD subunits are required for DSB repair, we performed several functional assays. Previous studies have reported roles for NuRD components in DSB repair by homologous recombination (HR) (Gong et al., 2015; Pan et al., 2012; Sun et al., 2016). This prompted us to test sensitivity for PARP inhibition, which is a measure of defective HR (McCabe et al., 2006). Knockdown of ZNF687, GATAD2A, or GATAD2B rendered cells highly sensitive to increasing concentrations of PARP inhibitor, suggesting a defect in HR (Figure 7C). We subsequently used the DR (direct repeat)-GFP reporter for HR activity, which measures the HR-dependent repair of a nuclease-induced DSB, resulting in the restoration of a functional *gfp* gene (Pierce et al., 1999). Flow-cytometric analysis of GFP fluorescence showed that knockdown of either CHD4 or ZMYND8 significantly reduced HR, although not to the same extent as core HR factor BRCA2 (Figure 7D). To validate these findings, we assessed the formation of RAD51 filaments in laser track experiments, since DNA-bound RAD51 mediates strand invasion and DNA transfer during HR. Analysis of irradiated cells showed that ZMYND8 knockout cells displayed moderately reduced recruitment of RAD51 compared to control cells, explaining the reduced HR efficiency (Figures 7E and 7F).

In summary, these findings suggest overlapping and unique roles of NuRD complex subunits in regulating HR-mediated DSB repair.

DISCUSSION

In this study, we have investigated the molecular nature and functional consequences of the interaction between ZMYND8 and the NuRD complex, which was previously reported to be

Figure 5. ZMYND8 Recruits GATAD2A-Containing NuRD Complex to Sites of DNA Damage

(A, B, D, F, H, J, and K) (Immuno)fluorescence microscopy on cells 5 min after treatment with a laser to induce DNA double-strand breaks. γH2AX indicates sites with DNA damage. (C, E, G, I, and L) Quantifications of (B), (D), (F), (H), and (K).

(A) Staining for endogenous ZMYND8 in control and ZMYND-KO cells.

(B and C) Staining of endogenous GATAD2A in control and ZMYND8-KO cells.

(D and E) Visualization of GFP-GATAD2B in control and ZMYND8-KO cells.

(F and G) Recruitment of MBD2-GFP in control, GATAD2A, or GATAD2B knockdown cells.

(H and I) MBD2-GFP enrichment in control and ZMYND8-KO cells.

(J) ZNF687-GFP accumulation upon laser-induced DNA damage.

(K and L) DNA damage recruitment of GFP-CHD4 in siLuc and siZNF687 cells.

Error bars indicate SEM. Two-tailed Student's t test p values: $^{**}p < 0.005$; $^{***}p < 5.10^{-6}$. See also Figure S4.

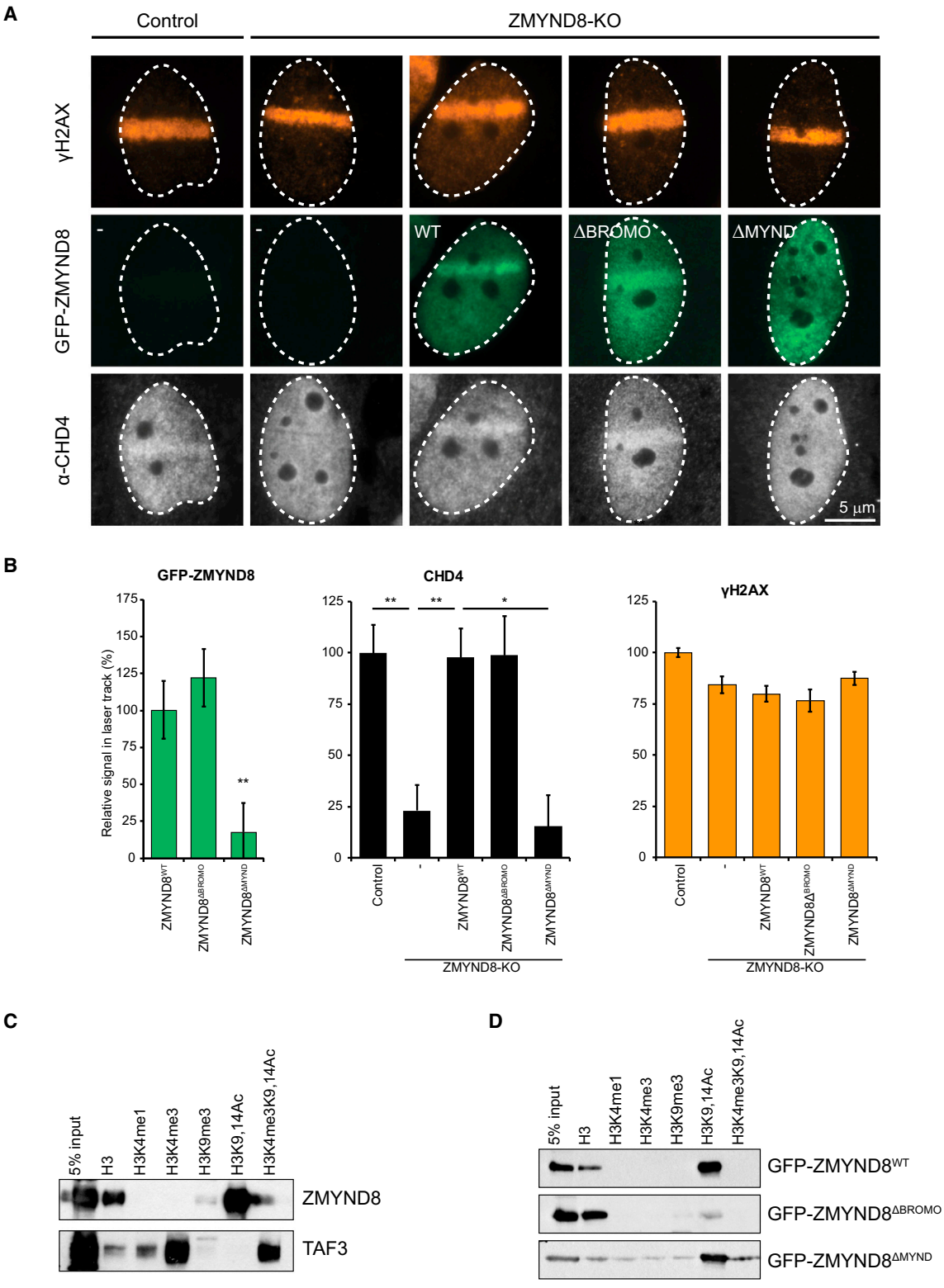

Figure 6. MYND Domain of ZMYND8 Is Required for Recruitment to Sites of DNA Damage

(A) (Immuno)fluorescence microscopy of cells 5 min after laser-induced DSBs showing endogenous CHD4 in control and ZMYND8-KO cells. Rescue effect of different GFP-fused ZMYND8 mutants is assessed.

(B) Quantification of (A). Error bars indicate SEM. Two-tailed Student's t test p values: *$p < 0.05$; **$p < 0.005$.

(legend continued on next page)

sub-stoichiometric (Smits et al., 2013). Our work revealed that ZMYND8 bridges the GATAD2A/NuRD complex to three ZNF proteins, ZNF532, ZNF592, and ZNF687, each of which contains a large number of putative DNA-binding ZNFs. Therefore, we hypothesized that this so-called Z3 module may serve to recruit GATAD2A/NuRD complexes to non-methylated target sites in the genome. Indeed, ChIP-seq for ZMYND8 and MBD3 revealed a substantial overlap of genome-wide binding sites, mostly active enhancers and promoters. However, ChIP-seq and ChIP-qPCR experiments in ZMYND8 knockout and rescue cell lines revealed that loss of ZMYND8 does not result in a loss of NuRD from its target genes. Based on these results, we hypothesized that the ZMYND8-GATAD2A/NuRD interaction is particularly important for an immediate recruitment to target genes that become induced or repressed following a stimulus. Future studies should shed further light on the kinetics and the importance, if any, of the ZMYND8-GATAD2A/NuRD interaction for NuRD-mediated transcription regulation in different cellular contexts. Support for the dynamic function of ZMYND8 is provided by its rapid poly(ADP-ribose)-dependent recruitment to DSBs. Once recruited, ZMYND8 contributes to the efficient recruitment of GATAD2A and CHD4, without an appreciable impact on GATAD2B. Efficient recruitment of MBD2 was also dependent on ZMYND8-GATAD2A, but not GATAD2B, suggesting a sequential recruitment model for these NuRD subunits through the ZMYND8-GATAD2A interaction. The genetic interdependencies of NuRD subunit recruitment to DSBs was often partial, arguing that several mechanistically distinct NuRD recruitment mechanisms contribute to its roles in the DSB response (Luijsterburg et al., 2012; Smeenk et al., 2010). We consistently observed defects in DSB repair by HR upon the loss of several distinct NuRD subunits, suggesting an important role for the NuRD complex in this repair pathway. Additional mechanistic studies will be required to unravel the unique and overlapping roles of individual NuRD subunits in DSB repair.

ChIP-seq experiments revealed a striking genome-wide correlation between ZMYND8/NuRD and active promoters and enhancers marked with H3K4me3 or H3K4me1 and histone acetylation marks (Figure 3B). ChIP-seq provides correlative data, and observed signals are derived from thousands of asynchronously dividing cells. However, expression analysis of ZMYND8/NuRD target genes revealed that NuRD bound genes tend to be highly expressed (Figure S3C). This positive correlation between NuRD and gene expression has also been observed by others (Shimbo et al., 2013; Whyte et al., 2012). Nevertheless, RNA-seq in ZMYND8 KO cells revealed a slight increase in expression of genes that are regulated by a nearby ZMYND8-bound (super) enhancer. This indicates that ZMYND8/NuRD mildly represses and, thus, fine-tunes expression of these genes, which is in agreement with two recent publications (Li et al., 2016; Shen et al., 2016). In any case, these observations force us to reconsider the textbook description of the NuRD complex as an exclusive transcriptionally repressive complex (Baymaz et al., 2015; Reynolds et al., 2013; Whyte et al., 2012). To investigate the exact function of the NuRD complex in regulating gene expression, time course experiments in which NuRD recruitment to target genes can be induced need to be designed. Such experiments will allow deciphering of the exact order of events and the transcriptional output following NuRD recruitment.

Finally, the mammalian NuRD complex contains a striking number of protein paralogues such as MBD2/3, MTA1/2/3, HDAC1/2, CHD3/4, and GATAD2A/B. These paralogues are vertebrate specific, as *Drosophila* NuRD only contains one GATAD2, CHD, MTA, and HDAC protein, for example. Apparently, during evolution, multiple NuRD subunit paralogues with distinct biological functions evolved. In this study, we have shown that the GATAD2A and GATAD2B paralogues define mutually exclusive NuRD subcomplexes. Furthermore, only GATAD2A interacts with the ZMYND8/Z3 module. Currently, it is not clear yet whether and which of the other NuRD subunit paralogues form hetero- or homomers and, thus, how many different functional compositions of the NuRD complex exist. In the future, paralogue-specific affinity purifications will surely shed more light on the biochemical and functional diversity of NuRD, which should be classified as a family of closely related protein complexes rather than a single biochemical entity.

EXPERIMENTAL PROCEDURES

Cloning

ZMYND8 isoform 17 was cloned into pEGFP-C3 (Clontech). This isoform is referred to as ZMYND8^{WT} throughout this study (Supplemental Information). GFP-ZMYND8^{WT} and GFP-ZMYND8^{dBROMO} mutant (isoform 1) constructs were kindly provided by Kyle Miller. GFP-GATAD2A was PCR amplified from a construct kindly provided by Dr. Imre Berger and cloned into the pEGFP-C3 vector. pcDNA5-FRT-TO-GFP constructs were created by Gateway cloning (Thermo Fisher Scientific). pCMV-mCHERRY-p66B was generously provided by Dr. Rainer Renkawitz and formed the template for PCR of GATAD2B. The ZMYND8 MYND domain was GST tagged in vector pRPN256NB.

Cell Culture and Generation of Stable Cell Lines

Hek293T, U2OS, HeLa Kyoto, or HeLa FRT-TO cells were grown according to standard protocols. Generation of stable inducible lines, shRNA-mediated knockdown lines, and CRISPR (clustered regularly interspaced short palindromic repeat) knockout cell lines, as well as details about SILAC culturing and siRNA transfections, can be found in the Supplemental Experimental Procedures. U2OS cells stably expressing GFP-CHD4 were previously described (Smeenk et al., 2010).

Nuclear Extract Preparation

Nuclear extracts (NEs) were prepared essentially as described previously (Dignam et al., 1983).

GFP Affinity Purification

GFP purifications were performed essentially as described previously (Baymaz et al., 2014).

MS

Liquid chromatography-tandem MS (LC-MS/MS) measurements were performed as described previously (Kloet et al., 2014).

(C) Histone peptide pull-down experiment in HeLa nuclear extracts, revealing enrichment of ZMYND8 and TAF3 on a variety of modified histone-tail peptides, as determined by western blotting.
(D) Histone peptide pull-down experiment in HeLa nuclear extracts expressing the indicated GFP-tagged ZMYND8 mutants.
See also Figure S4.

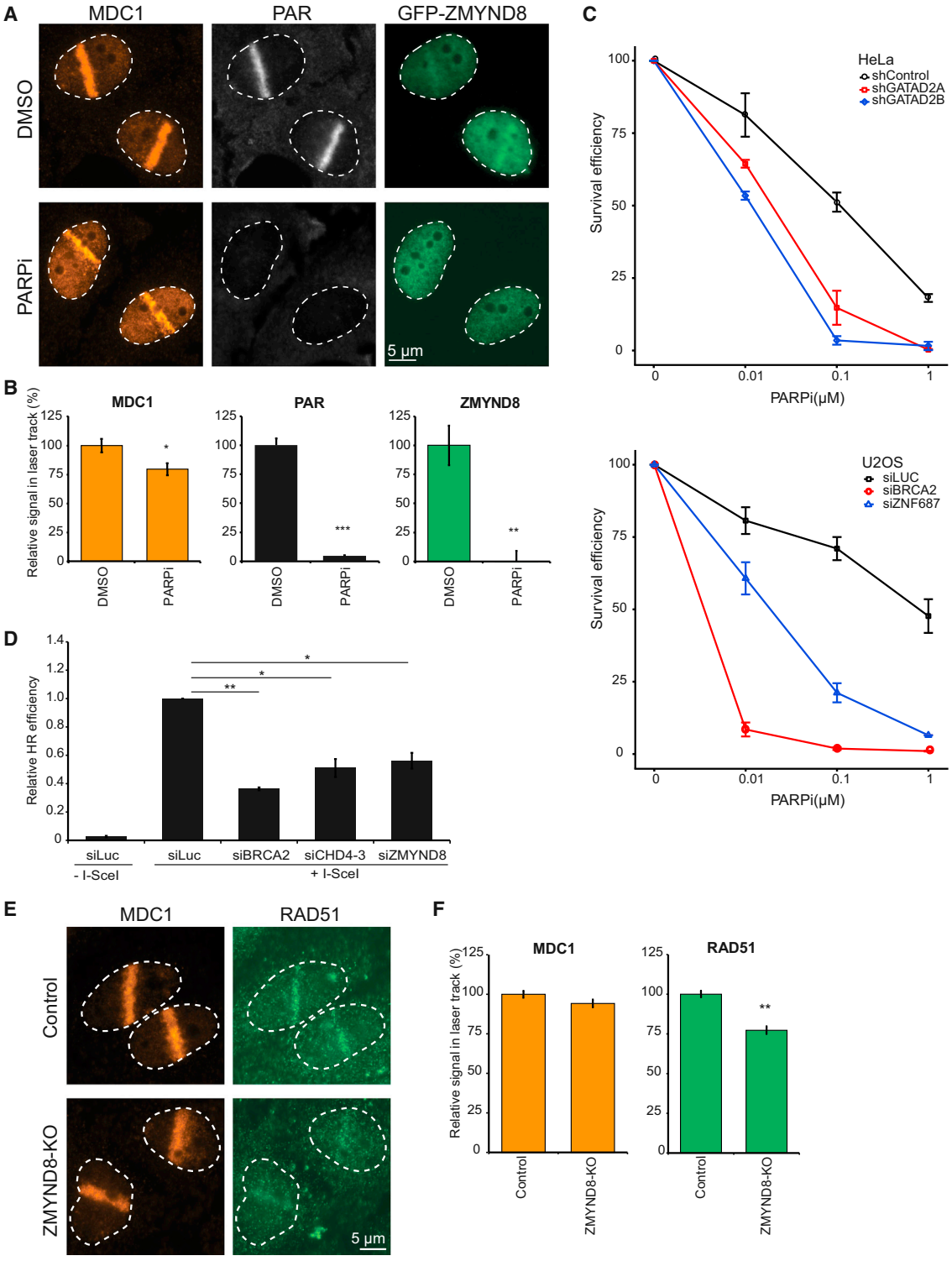

Figure 7. ZMYND8 and NuRD Function in a PARP-Dependent DNA Damage Pathway

(A) Visualization of GFP-ZMYND8 recruitment in DMSO- or PARPi-treated cells.

(B) Quantification of (A).

(C) Survival assays of GATAD2A and GATAD2B knockdown HeLa cells and siZNF687-treated U2OS cells. siBRCA2 is a positive control.

(legend continued on next page)

MS Data Analysis

Raw data were analyzed using the MaxQuant software package, Perseus, and R (Cox et al., 2014; Cox and Mann, 2008; Tyanova et al., 2016). Details about data analyses are described in the Supplemental Information. Processed MS data can be found in Table S1.

ChIP-Seq

Details about chromatin preparation and ChIP, such as antibodies, can be found in Supplemental Experimental Procedures. X-linking of cells was performed using disuccinimidyl glutarate (DSG) and formaldehyde. Library preparation was performed using the KAPA Kit and Nextflex adaptors. Purified DNA was analyzed by deep sequencing on the Illumina GAIIx or Illumina HiSeq2000 genome analyzers.

Library Sequencing and Data Analysis

Reads were mapped to hg19 (NCBI build 37) using BWA, allowing one mismatch. Peak-calling was performed with the MACS 2.0 tool. ZMYND8 peaks and their assigned target genes are listed in Table S2.

The Python package used for K-means clustering and generation of heatmaps and bandplots is available at http://simonvh.github.io/fluff/ (Georgiou and van Heeringen, 2016). R was used to generate bandplots.

Available RCOR1 ChIP-seq data in HeLa S3 (GSM1104353) were used to generate heatmaps (Zhang et al., 2013). DNA methylation was analyzed using ENCODE (Encyclopedia of DNA Elements) dataset GSM999337. The ChIP-seq datasets for H3K4me1, H3k27ac, DNase I, and P300 were retrieved from the ENCODE data repository site (http://genome.ucsc.edu/ENCODE/).

RNA-Seq

RNA was purified using the QIAGEN RNeasy Mini Kit. rRNA was removed using the Ribo-Zero rRNA Removal Kit (Illumina). cDNA was synthesized while retaining strand identity. The paired-end reads were aligned to hg19 using the Genomic Short-read Alignment Program (Wu and Watanabe, 2005), allowing one mismatch. Aligned reads were analyzed using BamTools API 1.0.2 (Barnett et al., 2011). Differential expression analysis was performed using the Cufflinks v2.1.1 package (Trapnell et al., 2010) by FPKM (fragments of kilobase per exon per million fragments mapped) on the human RefSeq transcript database (Pruitt et al., 2014).

UV-A Laser Micro-irradiation

Cells were grown on coverslips and sensitized with bromodeoxyuridine (BrdU). When required, cells were simultaneously induced with doxycycline. The growth medium was replaced by Leibovitz's L15 medium with 10% fetal calf serum (FCS) and penicillin-streptomycin (pen-strep), and cells were kept at 37°C. For micro-irradiation, the cells were treated with a pulsed nitrogen laser (16 Hz, 364 nm, Micropoint Ablation Laser System; Andor) that was focused through a Leica 40× HCX Plan Apo 1.25-0.75 oil-immersion objective. The laser output power was 72. On average, 50 cells were micro-irradiated (2 iterations per pixel) within 5 min, using Andor IQ software (Andor). For details, see Supplemental Information.

Histone Peptide Pull-Downs

Histone peptide pull-downs were performed as described previously (Vermeulen et al., 2010).

Cell-Cycle Profiling

For cell-cycle analysis, cells were fixed in 70% ethanol, followed by DNA staining with 50 μg/mL propidium iodide in the presence of RNase A (0.1 mg/ml) (Sigma). Cell sorting was performed on a BD LSR II flow cytometer (BD Biosciences) using BD FACSDiva Software (version 5.0.3; BD Biosciences). Quantifications were performed using Flowing Software.

Immunofluorescent Labeling and Image Acquisition

Immunofluoresecent labeling was carried out as described previously (Luijsterburg et al., 2012). Details can be found in the Supplemental Experimental Procedures.

Images were acquired on a Zeiss Axio Imager M2 wide-field fluorescence microscope using a 63× Plan Apo (1.4 NA) oil-immersion objective (Zeiss) and an HXP 120 metal halide lamp used for excitation. Images were recorded using ZEN 2012 software and quantified using ImageJ.

HR Assay

U2OS cells containing the DR-GFP reporter were used to measure the repair of I-SceI-induced DSBs by HR as described previously (Pierce et al., 1999). For more details, see Supplemental Experimental Procedures.

PARP Inhibitor Survival

U2OS cells were transfected with small interfering RNA (siRNA) and, after 48 hr, trypsinized, seeded, and exposed to PARP inhibitor KU-0058948 (AstraZeneca) at the indicated concentration. After 7 days, the cells were stained with methylene blue. Colonies containing more than 20 cells were scored.

Statistical Methods

The p values in SILAC-based GFP affinity purifications were calculated using significance B in Perseus. Specific interactors in LFQ-based GFP affinity purifications were determined using an adapted two-tailed Student's t test in the Perseus software (permutation-based false discovery rate [FDR] with 250 randomizations); s_0 and FDR are indicated in the graphs. For ChIP-qPCR and qRT-PCR, p values were determined using two-tailed Student's t tests on technical triplicates of one of the representative experiments. For micro-irradiation experiments, mean and SEM were determined based on more than 40 cells per condition divided over multiple experiments. The p values were calculated using two-tailed Student's t test.

ACCESSION NUMBERS

The accession number for raw and processed MS data reported in this paper is PXD: PXD003856. These data have been deposited in the ProteomeXchange Consortium via the PRIDE partner repository (Vizcaíno et al., 2016). The accession number for all high-throughput sequencing data reported in this paper is GEO: GSE79836.

SUPPLEMENTAL INFORMATION

Supplemental Information includes Supplemental Experimental Procedures, four figures, and two tables and can be found with this article online at http://dx.doi.org/10.1016/j.celrep.2016.09.037.

AUTHOR CONTRIBUTIONS

C.G.S. and M.V. conceived the project and wrote the manuscript, with input from all other authors. C.G.S. performed all MS and cloning experiments, as well as most ChIP and qRT-PCR experiments. M.S.L., W.W.W., and H.v.A. performed DNA damage experiments. R.M. and R.G.H.L. performed analysis of ChIP-seq and RNA-seq data, respectively. P.W.T.C.J. and H.R.V. assisted the MS experiments. R.R.E. and M.P.B. made CRISPR ZMYND8 knockout cell lines. F.M. performed the ZMYND8-GFP ChIP-seq. I.P., M.C.V.-A. and A.M. made stable cell lines. H.G.S., H.V.A., and M.V. supervised the project.

(D) Bar graph showing HR efficiency in siRNA-mediated knockdown cells as measured by a DR-GFP assay. The reporter cell line contains two dysfunctional *gfp* genes. Expression of I-SceI induces a DNA double-strand break, and repair of this break by homologous recombination leads to a functional *gfp* gene.
(E) Formation of RAD51 foci in control or ZMYND8-KO cells.
(F) Quantification of (E).
Error bars indicate SEM. Two-tailed Student's t test p values: *$p < 0.05$; **$p < 0.005$; ***$p < 5.10^{-6}$. See also Figure S4.

ACKNOWLEDGMENTS

We are grateful to Dr. Kyle Miller, Dr. Rainer Renkawitz, and Imre Berger for sharing constructs. We would like to thank Dr. Rehmann for advice and sharing of reagents. The authors thank the M.V. and Timmers groups for constructive discussions. C.G.S. would like to thank the NVBMB for financial support. M.V. is supported by the Netherlands Organisation for Scientific Research (NWO-VIDI (no. 864.09.003), the NWO Gravitation Program Cancer Genomics Netherlands), and the European Commission Framework Program FP7 project 4DCellFate (277899). I.P. thanks Anthony Hyman for support. The work of I.P. was supported by the European Community's Framework Program FP7 project MitoSys (241548). H.R.V. is financially supported by the NWO program Proteins@Work. M.S.L. is supported by NWO ALW-VENI and a LUMC research fellowship. H.v.A. receives financial support through an ERC-CoG grant.

Received: March 29, 2016
Revised: August 10, 2016
Accepted: September 13, 2016
Published: October 11, 2016

REFERENCES

Adhikary, S., Sanyal, S., Basu, M., Sengupta, I., Sen, S., Srivastava, D.K., Roy, S., and Das, C. (2016). Selective recognition of H3.1K36 dimethylation/H4K16 acetylation facilitates the regulation of all-trans-retinoic acid (ATRA)-responsive genes by putative chromatin reader ZMYND8. J. Biol. Chem. *291*, 2664–2681.

Allen, H.F., Wade, P.A., and Kutateladze, T.G. (2013). The NuRD architecture. Cell. Mol. Life Sci. *70*, 3513–3524.

Ansieau, S., and Leutz, A. (2002). The conserved Mynd domain of BS69 binds cellular and oncoviral proteins through a common PXLXP motif. J. Biol. Chem. *277*, 4906–4910.

Ansieau, S., and Sergeant, A. (2003). [BS69 and RACK7, a potential novel class of tumor suppressor genes]. Pathol. Biol. (Paris) *51*, 397–399.

Barnett, D.W., Garrison, E.K., Quinlan, A.R., Strömberg, M.P., and Marth, G.T. (2011). BamTools: a C++ API and toolkit for analyzing and managing BAM files. Bioinformatics *27*, 1691–1692.

Baymaz, H.I., Spruijt, C.G., and Vermeulen, M. (2014). Identifying nuclear protein-protein interactions using GFP affinity purification and SILAC-based quantitative mass spectrometry. Methods Mol. Biol. *1188*, 207–226.

Baymaz, H.I., Karemaker, I.D., and Vermeulen, M. (2015). Perspective on unraveling the versatility of 'co-repressor' complexes. Biochim. Biophys. Acta *1849*, 1051–1056.

Chou, D.M., Adamson, B., Dephoure, N.E., Tan, X., Nottke, A.C., Hurov, K.E., Gygi, S.P., Colaiácovo, M.P., and Elledge, S.J. (2010). A chromatin localization screen reveals poly (ADP ribose)-regulated recruitment of the repressive polycomb and NuRD complexes to sites of DNA damage. Proc. Natl. Acad. Sci. USA *107*, 18475–18480.

Cox, J., and Mann, M. (2008). MaxQuant enables high peptide identification rates, individualized p.p.b.-range mass accuracies and proteome-wide protein quantification. Nat. Biotechnol. *26*, 1367–1372.

Cox, J., Hein, M.Y., Luber, C.A., Paron, I., Nagaraj, N., and Mann, M. (2014). Accurate proteome-wide label-free quantification by delayed normalization and maximal peptide ratio extraction, termed MaxLFQ. Mol. Cell. Proteomics *13*, 2513–2526.

Dignam, J.D., Lebovitz, R.M., and Roeder, R.G. (1983). Accurate transcription initiation by RNA polymerase II in a soluble extract from isolated mammalian nuclei. Nucleic Acids Res. *11*, 1475–1489.

Eberl, H.C., Spruijt, C.G., Kelstrup, C.D., Vermeulen, M., and Mann, M. (2013). A map of general and specialized chromatin readers in mouse tissues generated by label-free interaction proteomics. Mol. Cell *49*, 368–378.

Fossey, S.C., Kuroda, S., Price, J.A., Pendleton, J.K., Freedman, B.I., and Bowden, D.W. (2000). Identification and characterization of PRKCBP1, a candidate RACK-like protein. Mamm. Genome *11*, 919–925.

Georgiou, G., and van Heeringen, S.J. (2016). fluff: exploratory analysis and visualization of high-throughput sequencing data. PeerJ *4*, e2209.

Gnanapragasam, M.N., Scarsdale, J.N., Amaya, M.L., Webb, H.D., Desai, M.A., Walavalkar, N.M., Wang, S.Z., Zu Zhu, S., Ginder, G.D., and Williams, D.C., Jr. (2011). p66Alpha-MBD2 coiled-coil interaction and recruitment of Mi-2 are critical for globin gene silencing by the MBD2-NuRD complex. Proc. Natl. Acad. Sci. USA *108*, 7487–7492.

Gong, F., Chiu, L.Y., Cox, B., Aymard, F., Clouaire, T., Leung, J.W., Cammarata, M., Perez, M., Agarwal, P., Brodbelt, J.S., et al. (2015). Screen identifies bromodomain protein ZMYND8 in chromatin recognition of transcription-associated DNA damage that promotes homologous recombination. Genes Dev. *29*, 197–211.

Hendrich, B., and Bird, A. (1998). Identification and characterization of a family of mammalian methyl-CpG binding proteins. Mol. Cell. Biol. *18*, 6538–6547.

Kateb, F., Perrin, H., Tripsianes, K., Zou, P., Spadaccini, R., Bottomley, M., Franzmann, T.M., Buchner, J., Ansieau, S., and Sattler, M. (2013). Structural and functional analysis of the DEAF-1 and BS69 MYND domains. PLoS ONE *8*, e54715.

Kloet, S.L., Baymaz, H.I., Makowski, M., Groenewold, V., Jansen, P.W., Berendsen, M., Niazi, H., Kops, G.J., and Vermeulen, M. (2014). Towards elucidating the stability, dynamics and architecture of the nucleosome remodeling and deacetylase complex by using quantitative interaction proteomics. FEBS J. *282*, 1774–1785.

Larsen, D.H., Poinsignon, C., Gudjonsson, T., Dinant, C., Payne, M.R., Hari, F.J., Rendtlew Danielsen, J.M., Menard, P., Sand, J.C., Stucki, M., et al. (2010). The chromatin-remodeling factor CHD4 coordinates signaling and repair after DNA damage. J. Cell Biol. *190*, 731–740.

Le Guezennec, X., Vermeulen, M., Brinkman, A.B., Hoeijmakers, W.A., Cohen, A., Lasonder, E., and Stunnenberg, H.G. (2006). MBD2/NuRD and MBD3/NuRD, two distinct complexes with different biochemical and functional properties. Mol. Cell. Biol. *26*, 843–851.

Li, N., Li, Y., Lv, J., Zheng, X., Wen, H., Shen, H., Zhu, G., Chen, T.Y., Dhar, S.S., Kan, P.Y., et al. (2016). ZMYND8 reads the dual histone mark H3K4me1-H3K14ac to antagonize the expression of metastasis-linked genes. Mol. Cell *63*, 470–484.

Liu, Y., Chen, W., Gaudet, J., Cheney, M.D., Roudaia, L., Cierpicki, T., Klet, R.C., Hartman, K., Laue, T.M., Speck, N.A., and Bushweller, J.H. (2007). Structural basis for recognition of SMRT/N-CoR by the MYND domain and its contribution to AML1/ETO's activity. Cancer Cell *11*, 483–497.

Luijsterburg, M.S., Acs, K., Ackermann, L., Wiegant, W.W., Bekker-Jensen, S., Larsen, D.H., Khanna, K.K., van Attikum, H., Mailand, N., and Dantuma, N.P. (2012). A new non-catalytic role for ubiquitin ligase RNF8 in unfolding higher-order chromatin structure. EMBO J. *31*, 2511–2527.

Malovannaya, A., Lanz, R.B., Jung, S.Y., Bulynko, Y., Le, N.T., Chan, D.W., Ding, C., Shi, Y., Yucer, N., Krenciute, G., et al. (2011). Analysis of the human endogenous coregulator complexome. Cell *145*, 787–799.

McCabe, N., Turner, N.C., Lord, C.J., Kluzek, K., Bialkowska, A., Swift, S., Giavara, S., O'Connor, M.J., Tutt, A.N., Zdzienicka, M.Z., et al. (2006). Deficiency in the repair of DNA damage by homologous recombination and sensitivity to poly(ADP-ribose) polymerase inhibition. Cancer Res. *66*, 8109–8115.

Pan, M.R., Hsieh, H.J., Dai, H., Hung, W.C., Li, K., Peng, G., and Lin, S.Y. (2012). Chromodomain helicase DNA-binding protein 4 (CHD4) regulates homologous recombination DNA repair, and its deficiency sensitizes cells to poly(ADP-ribose) polymerase (PARP) inhibitor treatment. J. Biol. Chem. *287*, 6764–6772.

Pierce, A.J., Johnson, R.D., Thompson, L.H., and Jasin, M. (1999). XRCC3 promotes homology-directed repair of DNA damage in mammalian cells. Genes Dev. *13*, 2633–2638.

Polo, S.E., Kaidi, A., Baskcomb, L., Galanty, Y., and Jackson, S.P. (2010). Regulation of DNA-damage responses and cell-cycle progression by the chromatin remodelling factor CHD4. EMBO J. *29*, 3130–3139.

Potts, R.C., Zhang, P., Wurster, A.L., Precht, P., Mughal, M.R., Wood, W.H., 3rd, Zhang, Y., Becker, K.G., Mattson, M.P., and Pazin, M.J. (2011). CHD5,

a brain-specific paralog of Mi2 chromatin remodeling enzymes, regulates expression of neuronal genes. PLoS ONE *6*, e24515.

Pruitt, K.D., Brown, G.R., Hiatt, S.M., Thibaud-Nissen, F., Astashyn, A., Ermolaeva, O., Farrell, C.M., Hart, J., Landrum, M.J., McGarvey, K.M., et al. (2014). RefSeq: an update on mammalian reference sequences. Nucleic Acids Res. *42*, D756–D763.

Reynolds, N., O'Shaughnessy, A., and Hendrich, B. (2013). Transcriptional repressors: multifaceted regulators of gene expression. Development *140*, 505–512.

Shen, H., Xu, W., Guo, R., Rong, B., Gu, L., Wang, Z., He, C., Zheng, L., Hu, X., Hu, Z., et al. (2016). Suppression of Enhancer Overactivation by a RACK7-Histone Demethylase Complex. Cell *165*, 331–342.

Shimbo, T., Du, Y., Grimm, S.A., Dhasarathy, A., Mav, D., Shah, R.R., Shi, H., and Wade, P.A. (2013). MBD3 localizes at promoters, gene bodies and enhancers of active genes. PLoS Genet. *9*, e1004028.

Smeenk, G., Wiegant, W.W., Vrolijk, H., Solari, A.P., Pastink, A., and van Attikum, H. (2010). The NuRD chromatin-remodeling complex regulates signaling and repair of DNA damage. J. Cell Biol. *190*, 741–749.

Smits, A.H., Jansen, P.W., Poser, I., Hyman, A.A., and Vermeulen, M. (2013). Stoichiometry of chromatin-associated protein complexes revealed by label-free quantitative mass spectrometry-based proteomics. Nucleic Acids Res. *41*, e28.

Spruijt, C.G., Bartels, S.J., Brinkman, A.B., Tjeertes, J.V., Poser, I., Stunnenberg, H.G., and Vermeulen, M. (2010). CDK2AP1/DOC-1 is a bona fide subunit of the Mi-2/NuRD complex. Mol. Biosyst. *6*, 1700–1706.

Spruijt, C.G., Gnerlich, F., Smits, A.H., Pfaffeneder, T., Jansen, P.W., Bauer, C., Münzel, M., Wagner, M., Müller, M., Khan, F., et al. (2013). Dynamic readers for 5-(hydroxy)methylcytosine and its oxidized derivatives. Cell *152*, 1146–1159.

Sun, Y., Yang, Y., Shen, H., Huang, M., Wang, Z., Liu, Y., Zhang, H., Tang, T.S., and Guo, C. (2016). iTRAQ-based chromatin proteomic screen reveals CHD4-dependent recruitment of MBD2 to sites of DNA damage. Biochem. Biophys. Res. Commun. *471*, 142–148.

Trapnell, C., Williams, B.A., Pertea, G., Mortazavi, A., Kwan, G., van Baren, M.J., Salzberg, S.L., Wold, B.J., and Pachter, L. (2010). Transcript assembly and quantification by RNA-Seq reveals unannotated transcripts and isoform switching during cell differentiation. Nat. Biotechnol. *28*, 511–515.

Tyanova, S., Temu, T., Sinitcyn, P., Carlson, A., Hein, M.Y., Geiger, T., Mann, M., and Cox, J. (2016). The Perseus computational platform for comprehensive analysis of (prote)omics data. Nat. Methods *13*, 731–740.

Varier, R.A., Carrillo de Santa Pau, E., van der Groep, P., Lindeboom, R.G., Matarese, F., Mensinga, A., Smits, A.H., Edupuganti, R.R., Baltissen, M.P., Jansen, P.W., et al. (2016). Recruitment of the mammalian histone modifying EMSY complex to target genes is regulated by ZNF131. J. Biol Chem. *291*, 7313–7324.

Vermeulen, M., Eberl, H.C., Matarese, F., Marks, H., Denissov, S., Butter, F., Lee, K.K., Olsen, J.V., Hyman, A.A., Stunnenberg, H.G., and Mann, M. (2010). Quantitative interaction proteomics and genome-wide profiling of epigenetic histone marks and their readers. Cell *142*, 967–980.

Vizcaíno, J.A., Csordas, A., del-Toro, N., Dianes, J.A., Griss, J., Lavidas, I., Mayer, G., Perez-Riverol, Y., Reisinger, F., Ternent, T., et al. (2016). 2016 update of the PRIDE database and its related tools. Nucleic Acids Res. *44* (*D1*), D447–D456.

Whyte, W.A., Bilodeau, S., Orlando, D.A., Hoke, H.A., Frampton, G.M., Foster, C.T., Cowley, S.M., and Young, R.A. (2012). Enhancer decommissioning by LSD1 during embryonic stem cell differentiation. Nature *482*, 221–225.

Wu, T.D., and Watanabe, C.K. (2005). GMAP: a genomic mapping and alignment program for mRNA and EST sequences. Bioinformatics *21*, 1859–1875.

Zhang, J., Bonasio, R., Strino, F., Kluger, Y., Holloway, J.K., Modzelewski, A.J., Cohen, P.E., and Reinberg, D. (2013). SFMBT1 functions with LSD1 to regulate expression of canonical histone genes and chromatin-related factors. Genes Dev. *27*, 749–766.

Cell Reports, Volume *17*

Supplemental Information

ZMYND8 Co-localizes with NuRD on Target Genes and Regulates Poly(ADP-Ribose)-Dependent Recruitment of GATAD2A/NuRD to Sites of DNA Damage

Cornelia G. Spruijt, Martijn S. Luijsterburg, Roberta Menafra, Rik G.H. Lindeboom, Pascal W.T.C. Jansen, Raghu Ram Edupuganti, Marijke P. Baltissen, Wouter W. Wiegant, Moritz C. Voelker-Albert, Filomena Matarese, Anneloes Mensinga, Ina Poser, Harmjan R. Vos, Hendrik G. Stunnenberg, Haico van Attikum, and Michiel Vermeulen

Figure S1

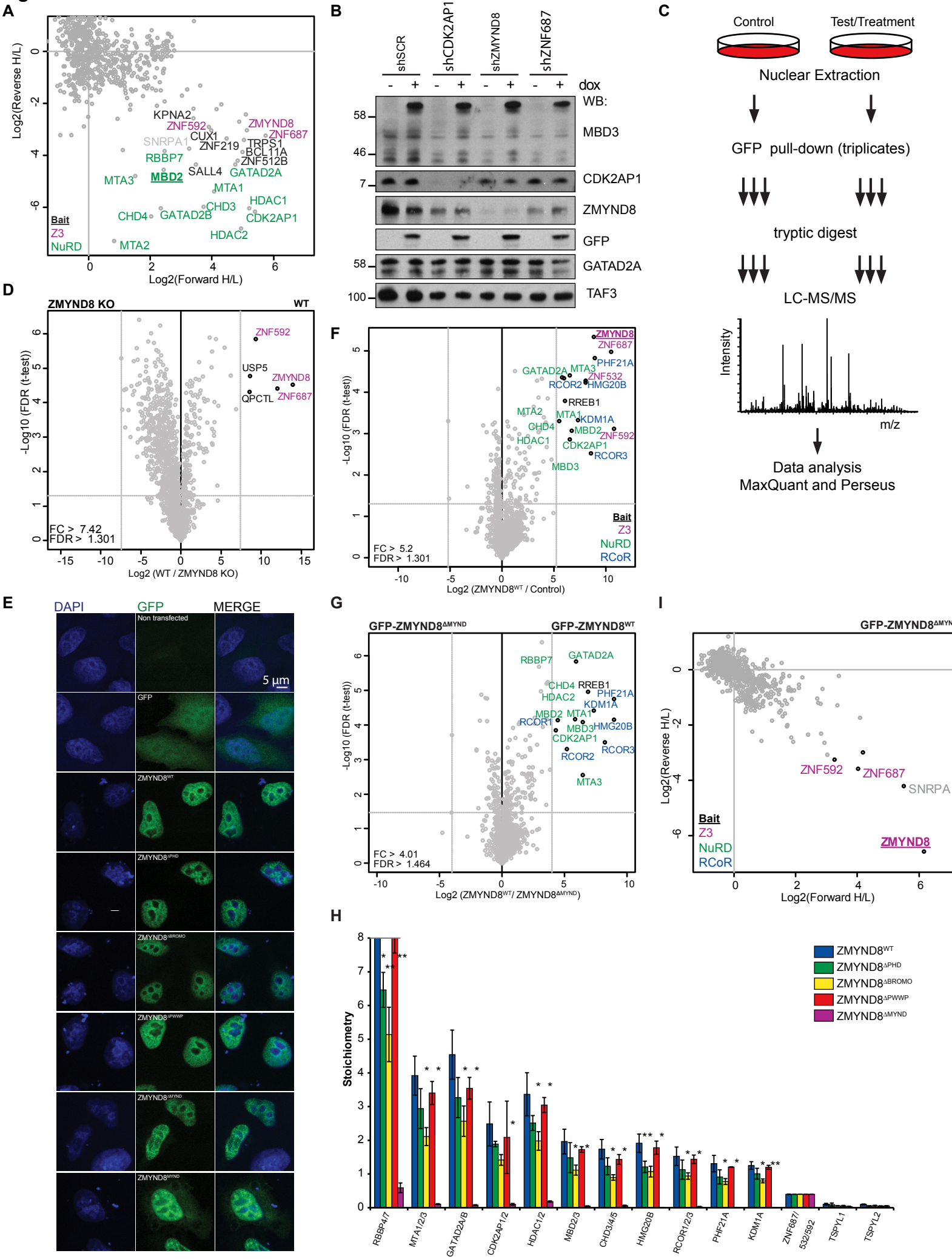
A
Log2(Reverse H/L)
Log2(Forward H/L)
KPNA2
ZNF592
ZMYND8
ZNF687
SNRPA1
CUX1
ZNF219
TRPS1
BCL11A
ZNF512B
RBBP7
SALL4
GATAD2A
MTA3
MBD2
MTA1
HDAC1
CHD3
CHD4
GATAD2B
CDK2AP1
HDAC2
MTA2
Bait
Z3
NuRD
B
shSCR
shCDK2AP1
shZMYND8
shZNF687
dox
WB:
MBD3
CDK2AP1
ZMYND8
GFP
GATAD2A
TAF3
C
Control
Test/Treatment
Nuclear Extraction
GFP pull-down (triplicates)
tryptic digest
LC-MS/MS
Intensity
m/z
Data analysis
MaxQuant and Perseus
D
ZMYND8 KO
WT
-Log10 (FDR (t-test))
Log2 (WT / ZMYND8 KO)
ZNF592
USP5
ZMYND8
QPCTL
ZNF687
FC > 7.42
FDR > 1.301
E
DAPI
GFP
MERGE
Non transfected
5 µm
GFP
ZMYND8WT
ZMYND8ΔPHD
ZMYND8ΔBROMO
ZMYND8ΔPWWP
ZMYND8ΔMYND
F
-Log10 (FDR (t-test))
Log2 (ZMYND8WT / Control)
ZMYND8
ZNF687
PHF21A
GATAD2A
MTA3
ZNF532
RCOR2
HMG20B
RREB1
MTA2
MTA1
KDM1A
CHD4
MBD2
ZNF592
HDAC1
CDK2AP1
RCOR3
MBD3
Bait
Z3
NuRD
RCoR
FC > 5.2
FDR > 1.301
G
GFP-ZMYND8ΔMYND
GFP-ZMYND8WT
-Log10 (FDR (t-test))
Log2 (ZMYND8WT/ ZMYND8ΔMYND)
RBBP7
GATAD2A
CHD4
RREB1
PHF21A
HDAC2
KDM1A
MBD2
MTA1
RCOR1
MBD3
HMG20B
CDK2AP1
RCOR3
RCOR2
MTA3
FC > 4.01
FDR > 1.464
H
Stoichiometry
ZMYND8WT
ZMYND8ΔPHD
ZMYND8ΔBROMO
ZMYND8ΔPWWP
ZMYND8ΔMYND
RBBP4/7
MTA1/2/3
GATAD2A/B
CDK2AP1/2
HDAC1/2
MBD2/3
CHD3/4/5
HMG20B
RCOR1/2/3
PHF21A
KDM1A
ZNF687/ 532/592
TSPYL1
TSPYL2
I
GFP-ZMYND8ΔMYND
Log2(Reverse H/L)
Log2(Forward H/L)
ZNF592
ZNF687
SNRPA1
Bait
Z3
NuRD
RCoR
ZMYND8

Figure S1: ZMYND8 mediates the interaction between the Z3 module and NuRD (related to Figure 1). A. Scatterplot of a SILAC-based GFP purification of MBD2-GFP. Z3 and NuRD subunits are indicated in magenta and green, respectively. **B.** Western blot analysis of the shRNA-mediated knock-down cell lines used in Figure 1C. **C.** Schematic overview of the workflow for LFQ-based GFP-affinity purifications. D**.** Volcano plot showing a direct comparison of proteins enriched with GFP-GATAD2A in WT (right) versus ZMYND8-KO cells (left). Analysis was performed simultaneously with Figure S2A and B. **E.** Confocal fluorescence microscopy shows nuclear localization of all ZMYND8-deletion mutant constructs in HeLa cells. Experiment performed simultaneously with Figure S2F. **F.** Volcano plot of LFQ purification of GFP-ZMYND8^{WT}. X-axis = Log2 (fold enrichment over negative control), Y-axis = –Log10(p-value). Z3, NuRD and BHC complex subunits are indicated in magenta, green and blue, respectively. **G.** Volcano plot showing a direct comparison of proteins enriched in GFP-ZMYND8^{WT} (right) compared to GFP-ZMYND8$^{\Delta MYND}$ (left). **H.** Stoichiometry determination of the interactors of different ZMYND8-deletion mutants. **I.** Scatterplot showing the results of a SILAC-based GFP-ZMYND8$^{\Delta MYND}$ purification.

Figure S2

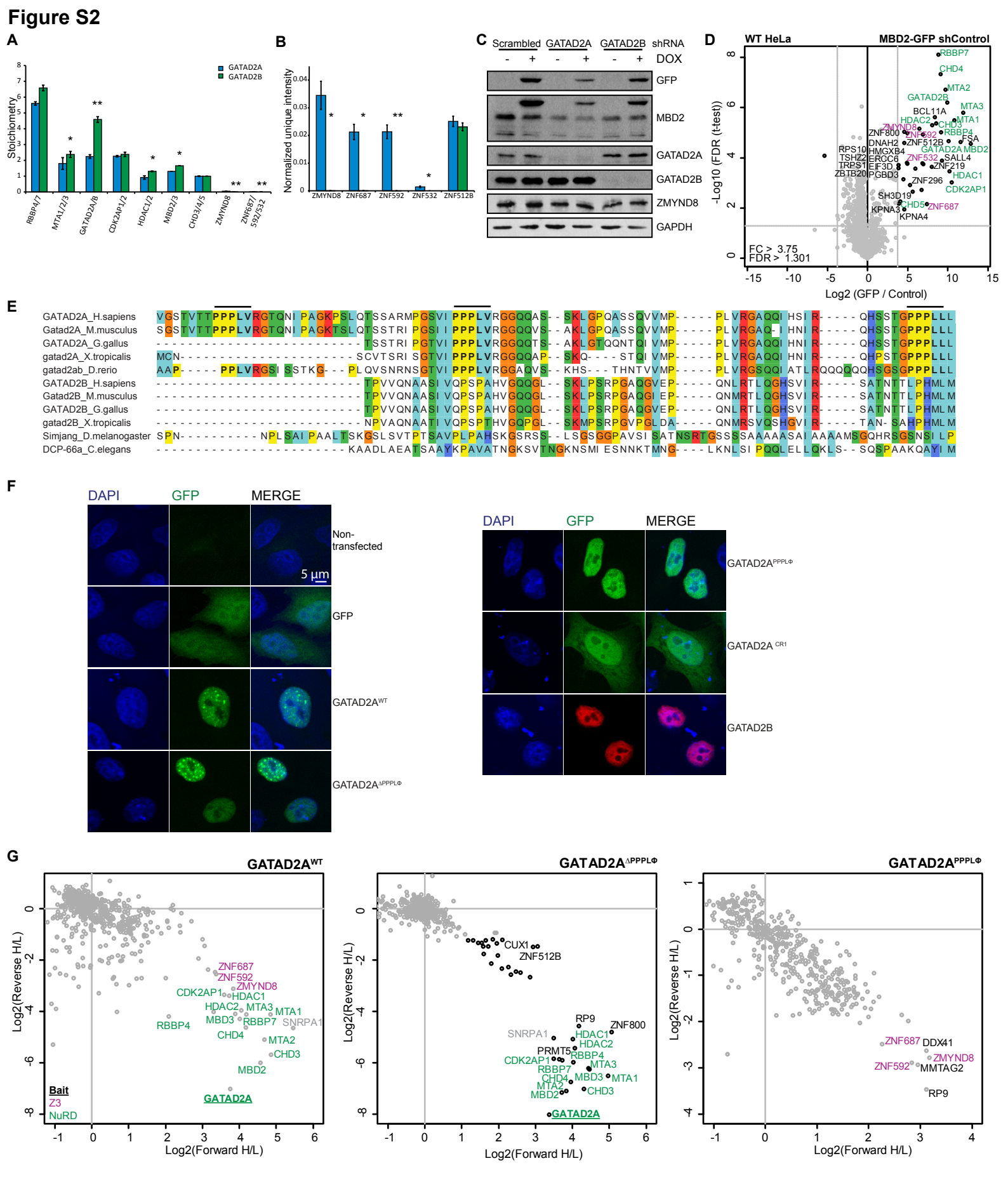
A
Stoichiometry
GATAD2A
GATAD2B
RBBP4/7
MTA1/2/3
GATAD2A/B
CDK2AP1/2
HDAC1/2
MBD2/3
CHD3/4/5
ZMYND8
ZNF687/ 592/532
B
Normalized unique intensity
ZMYND8
ZNF687
ZNF592
ZNF532
ZNF512B
C
Scrambled
GATAD2A
GATAD2B
shRNA
DOX
GFP
MBD2
GATAD2A
GATAD2B
ZMYND8
GAPDH
D
WT HeLa
MBD2-GFP shControl
-Log10 (FDR (t-test))
Log2 (GFP / Control)
FC > 3.75
FDR > 1.301
RBBP7
CHD4
MTA2
GATAD2B
MTA3
BCL11A
HDAC2
CHD3
MTA1
ZMYND8
RBBP4
ZNF800
ZNF592
FSA
DNAH2
ZNF512B
RPS10
HMGXB4
GATAD2A
MBD2
TSHZ2
ERCC6
ZNF532
SALL4
TRPS1
EIF3D
ZNF219
ZBTB20
PGBD3
HDAC1
ZNF296
CDK2AP1
SH3D19
HDS
ZNF687
KPNA3
KPNA4
E
GATAD2A_H.sapiens
Gatad2A_M.musculus
GATAD2A_G.gallus
gatad2A_X.tropicalis
gatad2ab_D.rerio
GATAD2B_H.sapiens
Gatad2B_M.musculus
GATAD2B_G.gallus
gatad2B_X.tropicalis
Simjang_D.melanogaster
DCP-66a_C.elegans
F
DAPI
GFP
MERGE
5 µm
Non-transfected
GFP
GATAD2A^WT
GATAD2A^ΔPPPLΦ
GATAD2A^PPPLΦ
GATAD2A CR1
GATAD2B
G
GATAD2A^WT
GATAD2A^ΔPPPLΦ
GATAD2A^PPPLΦ
Log2(Reverse H/L)
Log2(Forward H/L)
Bait
Z3
NuRD
ZNF687
ZNF592
ZMYND8
CDK2AP1
HDAC1
HDAC2
MTA3
MTA1
MBD3
RBBP7
SNRPA1
RBBP4
CHD4
MTA2
CHD3
MBD2
GATAD2A
CUX1
ZNF512B
RP9
ZNF800
SNRPA1
HDAC1
HDAC2
PRMT5
RBBP4
CDK2AP1
MTA3
RBBP7
CHD4
MBD3
MTA1
MTA2
CHD3
MBD2
GATAD2A
ZNF687
DDX41
ZMYND8
ZNF592
MMTAG2
RP9

Figure S2: ZMYND8 interacts with GATAD2A/NuRD (related to Figure 2). A. iBAQ-based stoichiometry determination of LFQ-based GFP-affinity purifications of GFP-GATAD2A and B (Figure 2A and B). GATAD2A values are the same as those shown in Figure 1F and G, since the analysis was performed simultaneously. **B.** Normalized unique intensities for NuRD-associated ZMYND8 and ZNF proteins in the GATAD2A and GATAD2B pull-downs. **C.** Western blot analyses of the shRNA-mediated knock down cell lines used in Figure 2D. **D.** Volcano plot of the LFQ-based GFP-purification of MBD2-GFP in the control shRNA cell line. The X-axis shows log2 of the fold enrichment in the specific versus the control purification. The Y-axis shows –Log10 of the p-value. Specific interactors are shown on the right. Z3 and NuRD complex subunits are indicated in magenta and green, respectively. **E.** Alignment of GATAD2A and B proteins from several (non-) vertebrate species. PPPLΦ motifs are indicated in **bold** and with a line on top. **F.** Confocal fluorescence microscopy to show subcellular localization of all GATAD2A mutant constructs in HeLa cells. GFP is the same as in Figure S1B, since microscopy was performed in one experiment. **G.** Scatterplots showing the results of SILAC-based GFP-affinity purifications of GFP-GATAD2A^{WT} (left), GFP-GATAD2A$^{\Delta PPPL\Phi}$ (middle), and GFP-GATAD2A$^{PPPL\Phi}$ (right).

Figure S3

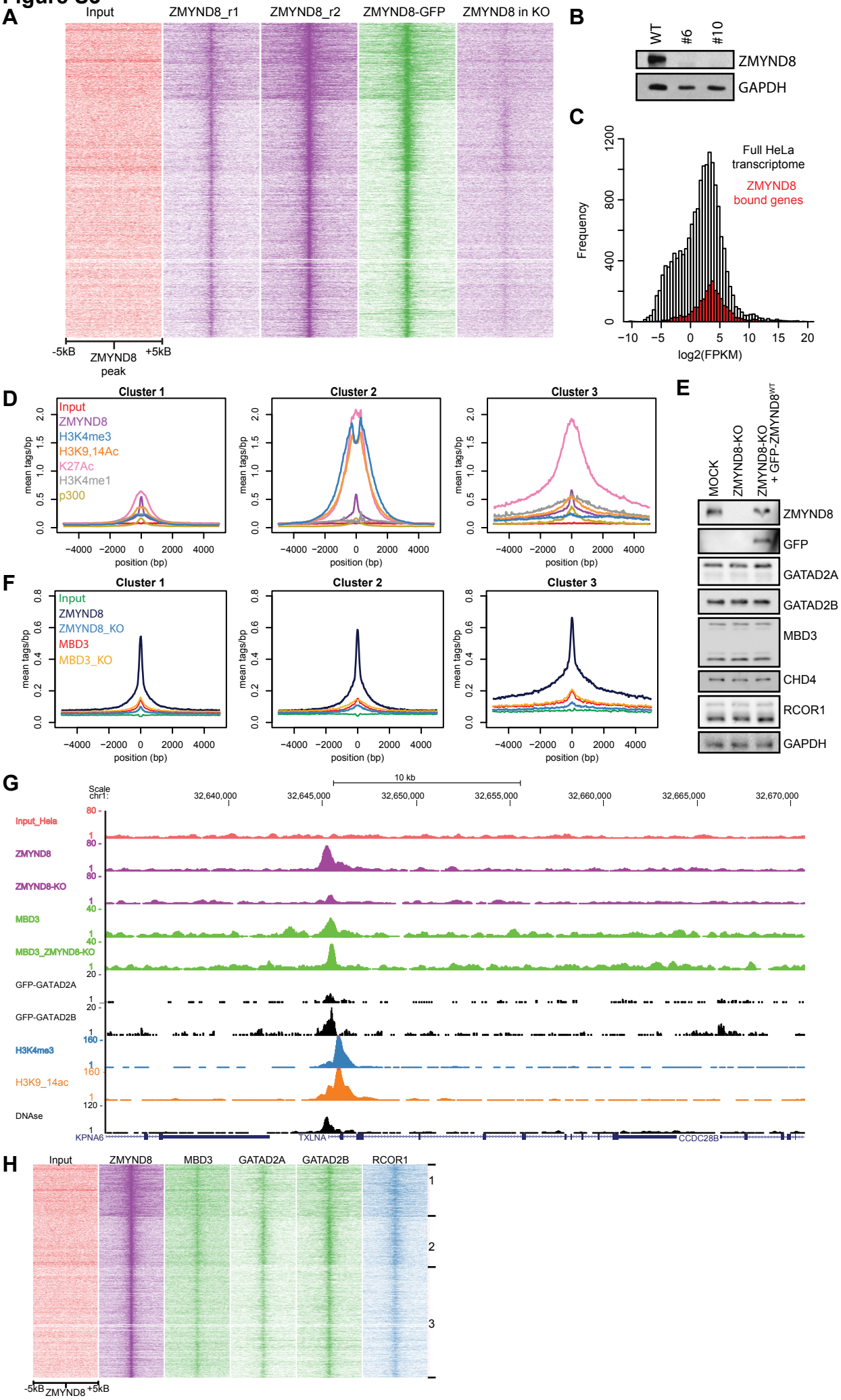
A
Input
ZMYND8_r1
ZMYND8_r2
ZMYND8-GFP
ZMYND8 in KO
-5kB
ZMYND8 peak
+5kB
B
WT
#6
#10
ZMYND8
GAPDH
C
Full HeLa transcriptome
ZMYND8 bound genes
Frequency
log2(FPKM)
D
Cluster 1
Cluster 2
Cluster 3
Input
ZMYND8
H3K4me3
H3K9,14Ac
K27Ac
H3K4me1
p300
mean tags/bp
position (bp)
E
MOCK
ZMYND8-KO
ZMYND8-KO + GFP-ZMYND8WT
ZMYND8
GFP
GATAD2A
GATAD2B
MBD3
CHD4
RCOR1
GAPDH
F
Cluster 1
Cluster 2
Cluster 3
Input
ZMYND8
ZMYND8_KO
MBD3
MBD3_KO
mean tags/bp
position (bp)
G
10 kb
Scale
chr1:
32,640,000
32,645,000
32,650,000
32,655,000
32,660,000
32,665,000
32,670,000
Input_Hela
ZMYND8
ZMYND8-KO
MBD3
MBD3_ZMYND8-KO
GFP-GATAD2A
GFP-GATAD2B
H3K4me3
H3K9_14ac
DNAse
KPNA6
TXLNA
CCDC28B
H
Input
ZMYND8
MBD3
GATAD2A
GATAD2B
RCOR1
-5kB
ZMYND8 peak
+5kB

Figure S3: Genome-wide ZMYND8 and NuRD binding (related to Figure 3 and 4). A. Heatmap centered on ZMYND8 peaks in replicate 2, showing input, two endogenous ZMYND8 ChIP replicates, a GFP-ChIP targeting ZMYND8-GFP and an endogenous ZMYND8 ChIP in ZMYND8 knock-out (KO) cells. **B.** Western blot showing two different ZMYND8 knock-out clones. **C.** Histogram showing expression levels of the total HeLa transcriptome. ZMYND8 bound genes are indicated in red. **D.** Bandplots centered on ZMYND8 peaks show co-occurrence of different histone marks with ZMYND8 in the three clusters. **E.** Western blot analyses of protein levels of NuRD subunits in the control, ZMYND8-KO or rescue cells that were used for the ChIP-qPCR experiment (Figure 4B). **F.** Bandplot analyses of ZMYND8 and MBD3 ChIPs in control and ZMYND8-KO cells. **G.** Screenshot of ZMYND8, MBD3, GATAD2A and GATAD2B ChIPs at the promoter of *TXLNA*. **H.** Heatmap centered on ZMYND8 peaks for MBD3, GFP-GATAD2A, GFP-GATAD2B and RCOR1 ChIP-seq data.

Figure S4

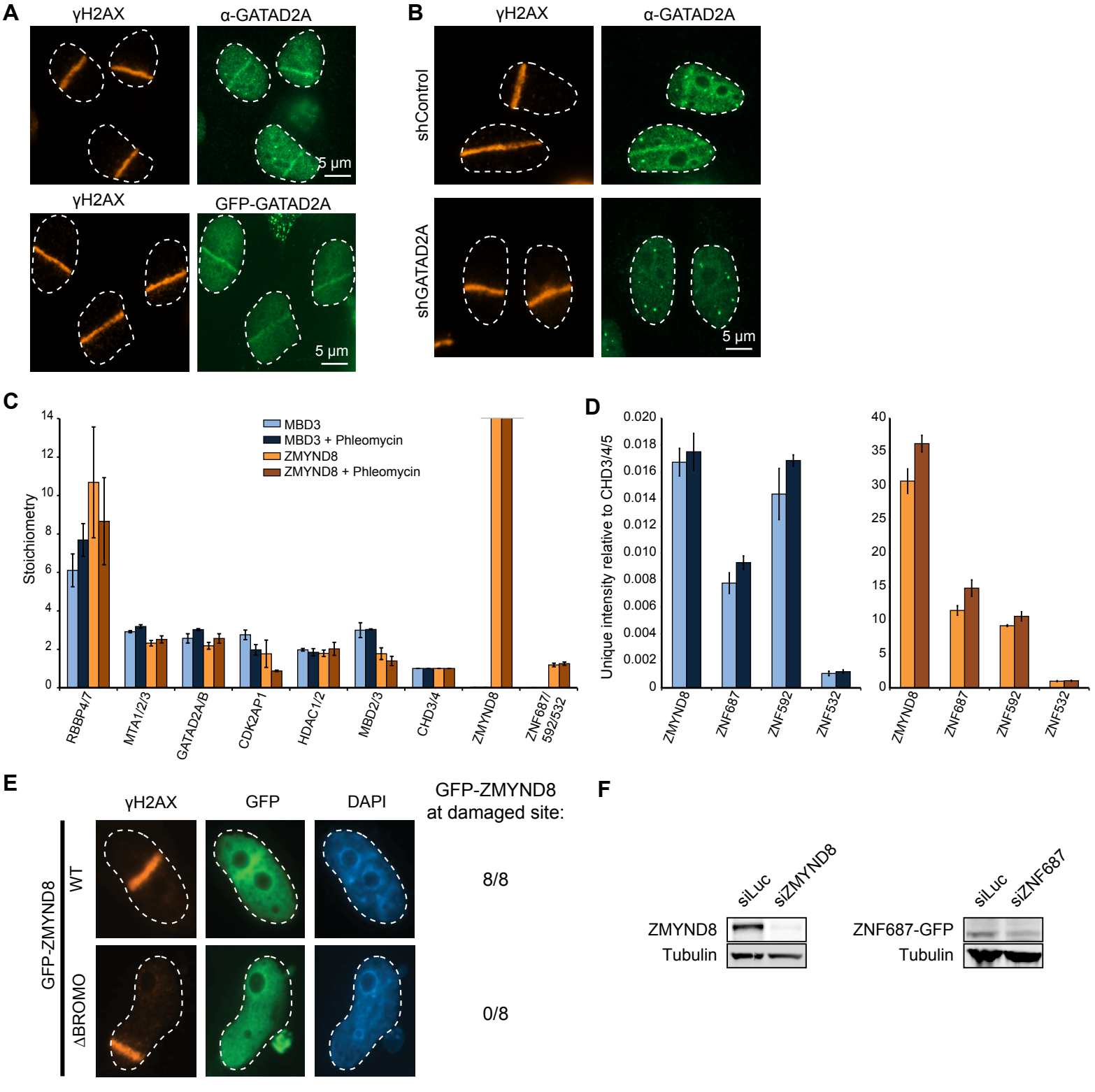
A
γH2AX
α-GATAD2A
5 μm
γH2AX
GFP-GATAD2A
5 μm
B
γH2AX
α-GATAD2A
shControl
shGATAD2A
5 μm
C
MBD3
MBD3 + Phleomycin
ZMYND8
ZMYND8 + Phleomycin
Stoichiometry
RBBP4/7
MTA1/2/3
GATAD2A/B
CDK2AP1
HDAC1/2
MBD2/3
CHD3/4
ZMYND8
ZNF687/ 592/532
D
Unique intensity relative to CHD3/4/5
ZMYND8
ZNF687
ZNF592
ZNF532
E
γH2AX
GFP
DAPI
GFP-ZMYND8 at damaged site:
GFP-ZMYND8
WT
ΔBROMO
8/8
0/8
F
siLuc
siZMYND8
ZMYND8
Tubulin
siLuc
siZNF687
ZNF687-GFP
Tubulin

Figure S4: ZMYND8 regulates NuRD recruitment to sites of DNA damage in a poly(ADP-ribose) dependent manner (related to figures 5, 6 and 7). A. (Immuno)fluorescence microscopy showing endogenous (top) and GFP-tagged (bottom) GATAD2A. DNA damage is indicated by staining for γH2Ax. **B.** GATAD2A antibody specificity test in control and shGATAD2A cells. **C.** Stoichiometry determination of LFQ-based GFP-purifications of MBD3 and ZMYND8 in the absence and presence of the DNA damage agent phleomycin. **D.** Normalized unique intensities for ZMYND8 and ZNF proteins in the experiment described in C. Error bars indicate standard deviation. Any observed differences are not significant according to a two-tailed student's t test p value <0.05. **E.** Fluorescence microscopy experiment investigating recruitment of GFP-ZMYND8 and GFP-ZMYND8ΔBROMO constructs (as used by Gong *et al.* (Gong et al., 2015)) to sites of DNA damage. **F.** Knock-down efficiency check for siRNAs targeting ZMYND8 (staining endogenous protein) and ZNF687 (tested in cells expressing ZNF687-GFP).

Supplemental Table 1: Processed Mass Spectrometry Data. Related to Figures 1, 2 and S4. Each tab of the excel file contains the processed data of a mass spectrometry experiment. Raw data was logarithmized, filtered, for LFQ experiments values were imputed and for SILAC experiments, p-values were calculated using significance B in Perseus.

Supplemental Table 2: ZMYND8 peak and gene lists. Related to Figure 3. The first tab contains a list of all peaks obtained for ZMYND8 in ChIP-seq. The second tab contains a list of genes that have a ZMYND8-bound promoter, enhancer, or both.

Supplemental Experimental Procedures

Cloning of constructs

ZMYND8 isoform 17 was PCR amplified from the Thermo Scientific cDNA clone 9052809/MHS1768-213246149 (Thermo Scientific) and ligated into pEGFP-C3. This isoform lacks some amino acid stretches, but no functional domains and is therefore referred to as ZMYND8^{WT} throughout this study. Deletion mutants were made by a 3-point ligation of two PCR products (sequences are shown below). GFP-GATAD2A was constructed by PCR from a codon-optimized construct kindly provided by Dr. Imre Berger and ligation into the pEGFP-C3 vector. pcDNA5-FRT-TO-MBD3-GFP, pcDNA5-FRT-TO-MBD2-GFP, pcDNA5FRT-TO-GFP-ZMYND8, GATAD2A and GATAD2B were created by Gateway® cloning (Thermo Scientific). The template for GATAD2B was a pCMV-mCHERRY-p66B generously provided by Dr. Rainer Renkawitz. For expression of GST-MYND, the same MYND construct was cloned into pRPN256NB.

Sequences of ZMYND8 and GATAD2A deletion contructs:

ZMYND8^{WT}:

MHPQSLAEEEIKTEQEVVEGMDISTRSKDPGSAERTAQKRKFPSPPHSSNGHSPQDTSTSPIKKKKKPGL
LNSNNKEQDGRNDFYCWVCHREGQVLCCELCPRVYHAKCLRLTSEPEGDWFCPECEKITVAECIETQS
KAMTMLTIEQLSYLLKFAIQKMKQPGTDAFQKPVPLEQHPDYAEYIFHPMDLCTLEKNAKKKMYGCTE
AFLADAKWILHNCIIYNGGNHKLTQIAKVVIKICEHEMNEIEVCPECYLAACQKRDNWFCEPCSNPHPL
VWAKLKGFPFWPAKALRDKDGQVDARFFGQHDRAWVPINNCYLMSKEIPFSVKKTKSIFNSAMQEME
VYVENIRRKFGVFNYSPFRTPYTPNSQYQMLLDPTNPSAGTAKIDKQEKVKLNFDMTASPKILMSKPVL
SGGTGRRISLSDMPRSPMSTNSSVHTGSDVEQDAEKKATSSHFSASEESMDFLDKSTASPASTKTGQAG
SLSGSPKPFSPQLSAPITTKTDKTSTTGSILNLNLDRSKAEMDLKELSESVQQQSTPVPLISPKRQIRSRFQL
NLDKTIESCKAQLGINEISEDVYTAVEHSDSEDSEKSDSSDSEYISDDEQKSKNEPEDTEDKEGCQMDKE
PSAVKKKPKPTNPVEIKEELKSTSPASEKADPGAVKDKASPEPEKDFSEKAKPSPHPIKDKLKGKDETDS
PTVHLGLDSDSESELVIDLGEDHSGREGRKNKKEPKEPSPKQDAVQQKEITQSPSTSTITLVTSTQSSPLV
TSSGSMSTLVSSVNADLPIATASADVAADIAKYTSKMMDAIKGTMTEIYNDLSKNTTGSTIAEIRRLRIEI
EKLQWLHQQELSEMKHNLELTMAEMRQSLEQERDRLIAEVKKQLELEKQQAVDETKKKQWCANCKK
EAIFYCCWNTSYCDYPCQQAHWPEHMKSCTQSATAPQQEADAEVNTETLNKSSQGSSSSTQSAPSETA
SASKEKETSAEKSKESGSTLDLSGSRETPSSILLGSNQGSDHSRSNKSSWSSSDEKRGSTRSDHNTSTSTK
SLLPKESRLDTFWD

ZMYND8$^{\Delta PHD}$:

MHPQSLAEEEIKTEQEVVEGMDISTRSKDPGSAERTAQKRKFPSPPHSSNGHSPQDTSTSPIKKKKKPGL
LNSNNKEQSTVAECIETQSKAMTMLTIEQLSYLLKFAIQKMKQPGTDAFQKPVPLEQHPDYAEYIFHPM
DLCTLEKNAKKKMYGCTEAFLADAKWILHNCIIYNGGNHKLTQIAKVVIKICEHEMNEIEVCPECYLAA
CQKRDNWFCEPCSNPHPLVWAKLKGFPFWPAKALRDKDGQVDARFFGQHDRAWVPINNCYLMSKEIP
FSVKKTKSIFNSAMQEMEVYVENIRRKFGVFNYSPFRTPYTPNSQYQMLLDPTNPSAGTAKIDKQEKVK
LNFDMTASPKILMSKPVLSGGTGRRISLSDMPRSPMSTNSSVHTGSDVEQDAEKKATSSHFSASEESMDF
LDKSTASPASTKTGQAGSLSGSPKPFSPQLSAPITTKTDKTSTTGSILNLNLDRSKAEMDLKELSESVQQQ
STPVPLISPKRQIRSRFQLNLDKTIESCKAQLGINEISEDVYTAVEHSDSEDSEKSDSSDSEYISDDEQKSK
NEPEDTEDKEGCQMDKEPSAVKKKPKPTNPVEIKEELKSTSPASEKADPGAVKDKASPEPEKDFSEKAK
PSPHPIKDKLKGKDETDSPTVHLGLDSDSESELVIDLGEDHSGREGRKNKKEPKEPSPKQDAVQQKEITQ
SPSTSTITLVTSTQSSPLVTSSGSMSTLVSSVNADLPIATASADVAADIAKYTSKMMDAIKGTMTEIYNDL
SKNTTGSTIAEIRRLRIEIEKLQWLHQQELSEMKHNLELTMAEMRQSLEQERDRLIAEVKKQLELEKQQ
AVDETKKKQWCANCKKEAIFYCCWNTSYCDYPCQQAHWPEHMKSCTQSATAPQQEADAEVNTETLN
KSSQGSSSSTQSAPSETASASKEKETSAEKSKESGSTLDLSGSRETPSSILLGSNQGSDHSRSNKSSWSSSD
EKRGSTRSDHNTSTSTKSLLPKESRLDTFWD

ZMYND8$^{\Delta BROMO}$:

MHPQSLAEEEIKTEQEVVEGMDISTRSKDPGSAERTAQKRKFPSPPHSSNGHSPQDTSTSPIKKKKKPGL
LNSNNKEQDGRNDFYCWVCHREGQVLCCELCPRVYHAKCLRLTSEPEGDWFCPECEKITVAECIETQS
KAMTMLTIEQLSYLLKFAIQSTAKVVIKICEHEMNEIEVCPECYLAACQKRDNWFCEPCSNPHPLVWAK
LKGFPFWPAKALRDKDGQVDARFFGQHDRAWVPINNCYLMSKEIPFSVKKTKSIFNSAMQEMEVYVE
NIRRKFGVFNYSPFRTPYTPNSQYQMLLDPTNPSAGTAKIDKQEKVKLNFDMTASPKILMSKPVLSGGT
GRRISLSDMPRSPMSTNSSVHTGSDVEQDAEKKATSSHFSASEESMDFLDKSTASPASTKTGQAGSLSGS
PKPFSPQLSAPITTKTDKTSTTGSILNLNLDRSKAEMDLKELSESVQQQSTPVPLISPKRQIRSRFQLNLDK
TIESCKAQLGINEISEDVYTAVEHSDSEDSEKSDSSDSEYISDDEQKSKNEPEDTEDKEGCQMDKEPSAV
KKKPKPTNPVEIKEELKSTSPASEKADPGAVKDKASPEPEKDFSEKAKPSPHPIKDKLKGKDETDSPTVH
LGLDSDSESELVIDLGEDHSGREGRKNKKEPKEPSPKQDAVQQKEITQSPSTSTITLVTSTQSSPLVTSSGS
MSTLVSSVNADLPIATASADVAADIAKYTSKMMDAIKGTMTEIYNDLSKNTTGSTIAEIRRLRIEIEKLQ
WLHQQELSEMKHNLELTMAEMRQSLEQERDRLIAEVKKQLELEKQQAVDETKKKQWCANCKKEAIF
YCCWNTSYCDYPCQQAHWPEHMKSCTQSATAPQQEADAEVNTETLNKSSQGSSSSTQSAPSETASASK
EKETSAEKSKESGSTLDLSGSRETPSSILLGSNQGSDHSRSNKSSWSSSDEKRGSTRSDHNTSTSTKSLLP
KESRLDTFWD

ZMYND8$^{\Delta PWWP}$:

MHPQSLAEEEIKTEQEVVEGMDISTRSKDPGSAERTAQKRKFPSPPHSSNGHSPQDTSTSPIKKKKKPGL
LNSNNKEQDGRNDFYCWVCHREGQVLCCELCPRVYHAKCLRLTSEPEGDWFCPECEKITVAECIETQS
KAMTMLTIEQLSYLLKFAIQKMKQPGTDAFQKPVPLEQHPDYAEYIFHPMDLCTLEKNAKKKMYGCTE
AFLADAKWILHNCIIYNGGNHKLTQIAKVVIKICEHEMNEIEVCPECYLAACQKRDNWFCEPCSSTKSIF
NSAMQEMEVYVENIRRKFGVFNYSPFRTPYTPNSQYQMLLDPTNPSAGTAKIDKQEKVKLNFDMTASP
KILMSKPVLSGGTGRRISLSDMPRSPMSTNSSVHTGSDVEQDAEKKATSSHFSASEESMDFLDKSTASPA
STKTGQAGSLSGSPKPFSPQLSAPITTKTDKTSTTGSILNLNLDRSKAEMDLKELSESVQQQSTPVPLISPK
RQIRSRFQLNLDKTIESCKAQLGINEISEDVYTAVEHSDSEDSEKSDSSDSEYISDDEQKSKNEPEDTEDK
EGCQMDKEPSAVKKKPKPTNPVEIKEELKSTSPASEKADPGAVKDKASPEPEKDFSEKAKPSPHPIKDKL
KGKDETDSPTVHLGLDSDSESELVIDLGEDHSGREGRKNKKEPKEPSPKQDAVQQKEITQSPSTSTITLV
TSTQSSPLVTSSGSMSTLVSSVNADLPIATASADVAADIAKYTSKMMDAIKGTMTEIYNDLSKNTTGSTI
AEIRRLRIEIEKLQWLHQQELSEMKHNLELTMAEMRQSLEQERDRLIAEVKKQLELEKQQAVDETKKK
QWCANCKKEAIFYCCWNTSYCDYPCQQAHWPEHMKSCTQSATAPQQEADAEVNTETLNKSSQGSSSS
TQSAPSETASASKEKETSAEKSKESGSTLDLSGSRETPSSILLGSNQGSDHSRSNKSSWSSSDEKRGSTRS
DHNTSTSTKSLLPKESRLDTFWD

ZMYND8$^{\Delta MYND}$:

MHPQSLAEEEIKTEQEVVEGMDISTRSKDPGSAERTAQKRKFPSPPHSSNGHSPQDTSTSPIKKKKKPGL
LNSNNKEQDGRNDFYCWVCHREGQVLCCELCPRVYHAKCLRLTSEPEGDWFCPECEKITVAECIETQS
KAMTMLTIEQLSYLLKFAIQKMKQPGTDAFQKPVPLEQHPDYAEYIFHPMDLCTLEKNAKKKMYGCTE
AFLADAKWILHNCIIYNGGNHKLTQIAKVVIKICEHEMNEIEVCPECYLAACQKRDNWFCEPCSNPHPL
VWAKLKGFPFWPAKALRDKDGQVDARFFGQHDRAWVPINNCYLMSKEIPFSVKKTKSIFNSAMQEME
VYVENIRRKFGVFNYSPFRTPYTPNSQYQMLLDPTNPSAGTAKIDKQEKVKLNFDMTASPKILMSKPVL
SGGTGRRISLSDMPRSPMSTNSSVHTGSDVEQDAEKKATSSHFSASEESMDFLDKSTASPASTKTGQAG
SLSGSPKPFSPQLSAPITTKTDKTSTTGSILNLNLDRSKAEMDLKELSESVQQQSTPVPLISPKRQIRSRFQL
NLDKTIESCKAQLGINEISEDVYTAVEHSDSEDSEKSDSSDSEYISDDEQKSKNEPEDTEDKEGCQMDKE
PSAVKKKPKPTNPVEIKEELKSTSPASEKADPGAVKDKASPEPEKDFSEKAKPSPHPIKDKLKGKDETDS
PTVHLGLDSDSESELVIDLGEDHSGREGRKNKKEPKEPSPKQDAVQQKEITQSPSTSTITLVTSTQSSPLV
TSSGSMSTLVSSVNADLPIATASADVAADIAKYTSKMMDAIKGTMTEIYNDLSKNTTGSTIAEIRRLRIEI
EKLQWLHQQELSEMKHNLELTMAEMRQSLEQERDRLIAEVKKQLELEKQQAVDETKKKSTQSATAPQ
QEADAEVNTETLNKSSQGSSSSTQSAPSETASASKEKETSAEKSKESGSTLDLSGSRETPSSILLGSNQGS
DHSRSNKSSWSSSDEKRGSTRSDHNTSTSTKSLLPKESRLDTFWD

ZMYND8^{MYND}:

IKKKKKKLIKKKKKGSTIAEIRRLRIEIEKLQWLHQQELSEMKHNLELTMAEMRQSLEQERDRLIAEVK
KQLELEKQQAVDETKKKQWCANCKKEAIFYCCWNTSYCDYPCQQAHWPEHMKSCTQSATAPQQEAD
AEVNTETLNKSSQGSSSSTQSAPSETASASKEKETSAEKSKESGSTLDLSGSRETPSSILLGSNQGSDHSRS
NKSSWSSSDEKRGSTRSDNTSTSTKSLLPKESRLDTFWD

GATAD2A^{WT}:
MTEEACRTRSQKRALERDPTEDDVESKKIKMERGLLASDLNTDGDMRVTPEPGAGPTQGLLRATEATA
MAMGRGEGLVGDGPVDMRTSHSDMKSERRPPSPDVIVLSDNEQPSSPRVNGLTTVALKETSTEALMKS
SPEERERMIKQLKEELRLEEAKLVLLKKLRQSQIQKEATAQKPTGSVGSTVTTPPPLVRGTQNIPAGKPS
LQTSSARMPGSVIPPPLVRGGQQASSKLGPQASSQVVMPPLVRGAQQIHSIRQHSSTGPPPLLLAPRASVP
SVQIQGQRIIQQGLIRVANVPNTSLLVNIPQPTPASLKGTTATSAQANSTPTSVASVVTSAESPASRQAAA
KLALRKQLEKTLLEIPPPKPPAPEMNFLPSAANNEFIYLVGLEEVVQNLLETQGRMSAATVLSREPYMC
AQCKTDFTCRWREEKSGAIMCENCMTTNQKKALKVEHTSRLKAAFVKALQQEQEIEQRLLQQGTAPA
QAKAEPTAAPHPVLKQVIKPRRKLAFRSGEARDWSNGAVLQASSQLSRGSATTPRGVLHTFSPSPKLQN
SASATALVSRTGRHSERTVSAGKGSATSNWKKTPLSTGGTLAFVSPSLAVHKSSSAVDRQREYLLDMIP
PRSIPQSATWK

GATAD2A$^{\Delta PPPL\Phi}$:
MTEEACRTRSQKRALERDPTEDDVESKKIKMERGLLASDLNTDGDMRVTPEPGAGPTQGLLRATEATA
MAMGRGEGLVGDGPVDMRTSHSDMKSERRPPSPDVIVLSDNEQPSSPRVNGLTTVALKETSTEALMKS
SPEERERMIKQLKEELRLEEAKLVLLKKLRQSQIQKEATAQKPTGSVSTSVASVVTSAESPASRQAAAKL
ALRKQLEKTLLEIPPPKPPAPEMNFLPSAANNEFIYLVGLEEVVQNLLETQGRMSAATVLSREPYMCAQ
CKTDFTCRWREEKSGAIMCENCMTTNQKKALKVEHTSRLKAAFVKALQQEQEIEQRLLQQGTAPAQA
KAEPTAAPHPVLKQVIKPRRKLAFRSGEARDWSNGAVLQASSQLSRGSATTPRGVLHTFSPSPKLQNSA
SATALVSRTGRHSERTVSAGKGSATSNWKKTPLSTGGTLAFVSPSLAVHKSSSAVDRQREYLLDMIPPR
SIPQSATWK

GATAD2A$^{PPPL\Phi}$:
LKKKRRQLAGSVGSTVTTPPPLVRGTQNIPAGKPSLQTSSARMPGSVIPPPLVRGGQQASSKLGPQASSQ
VVMPPLVRGAQQIHSIRQHSSTGPPPLLLAPRASVPSVQIQGQRIIQQGLIRVAA

GATAD2A^{CR1}:
LKKKRRQLAVNGLTTVALKETSTEALMKSSPEERERMIKQLKEELRLEEAKLVLLKKLRQSQIQKEATA
QKPTGSV

Cell culture and transfection
Hek293T, Hela Kyoto or HeLa FRT-TO cells were grown in Dulbecco's modified essential medium (DMEM) containing 4.5 g/ml glucose, 10% FBS and 1% penicillin/streptomycin. For all HeLa FRT-TO lines 5 µg/ml blasticidin was added to the medium and for HeLa FRT-TO cells containing an inducible gene this was supplemented with 0.25 mg/ml hygromycin.

For SILAC experiments, cells were cultured in SILAC DMEM plus 10% dialyzed serum, 1% glutamine, 1% penicillin/streptomycin, and 30 µg/ml of either light arginine (R0) and 73 µg/ml lysine (K0) OR 73 µg/ml heavy lysine (K8) and 30 µg/ml arginine (R10) for at least 8 cell divisions. Cells were then expanded and transfected using PEI. After 20 hours, cells were harvested for nuclear extract preparation.

The stable inducible GFP-ZMYND8, GFP-GATAD2A, GFP-GATAD2B, MBD2-GFP and MBD3-GFP HeLa FRT cell lines were made by co-transfection of pcDNA5-FRT-TO-MBD3-GFP and pOG44 containing the flippase into HeLa FRT-TO cells, after 2 days followed by hygromycin selection.

shRNA knock down

Cos 7 cells grown in F12 medium + 10% serum were transfected with pLKO vectors containing shRNA in addition to the lentiviral packaging plasmids. The medium was refreshed after 24 hours and the medium of the next 48 hours was concentrated and used to tranduce the target HeLa cells in the presence of polybrene. After 24 hours, puromycin selection was applied and for some shRNAs, monoclonal lines were selected. Knock-down efficiencies were checked by RT-qPCR and, when possible, by western blot.

Generation of a CRISPR/Cas9 mediated knock-out cell line
Complimentary oligo's coding for a guide RNA targeting exon 4 of ZMYND8 were annealed and cloned into pSpCas9(BB)-2A-Puro (PX459) (Addgene 48139) (Ran et al., 2013) using conventional cloning. The resulting construct was sequenced verified and transfected. Two days after the transfection, cells were cultured under Puromycin selection for 48 hours, after which monoclonal cell lines were selected and sequence analyzed. The guide-RNA sequence was: AGATGTATTCCGCATAGTCAGGG**.**

Transfections
All siRNA transfections (see list of siRNA sequences) were performed with 40 nM siRNA duplexes using Lipofectamine RNAiMAX (Invitrogen). Cells were transfected twice with siRNAs at 0 and 36 hrs and were typically analyzed 60 hrs after the first transfection.

List of siRNA sequences

Target	Sequence
BRCA2	GAAGAAUGCAGGUUUAAUA
CHD4-2	CAAAGGUGCUGCUGAUGUA
CHD4-3	GAGCGGCAGUUCUUUGUGA
Luciferase (Luc)	CGUACGCGGAAUACUUCGA
ZMYND8 (smartpool)	D-017354-1: CAAAGAAGGUUGUCAGAUG D-017354-2: UAAAUGAAAUCUCGGAAGA D-017354-3: CAAGAGCUCUCCGAAAUGA D-017354-4: CGAAGUAUGUCCAGAAUGU
ZNF687 (smartpool)	D-007036-1: GCCCUAAGAUGAUUGCUAA D-007036-2: GGAGGAGACUGCUGGGAAA D-007036-3: GAAGGAGCAUGGCAAGUCA D-007036-4: UGACAUCCCUGACAUUGAU

GFP affinity purification

Nuclear extracts were derived from HeLa cells, either transiently or stably expressing the GFP-tagged constructs. Nuclear extracts were prepared according to (Dignam et al., 1983).

GFP affinity purifications were performed essentially as described by (Baymaz et al., 2014). Purifications coupled to label-free based quantification were always performed in triplicates. SILAC-based pull-downs were always performed in a 'forward' and 'reverse' manner (label-swap). Either wildtype cells or blocked agarose-beads (Chromotek) were used as a negative control for the GFP-purifications performed with GFP-trap beads (Chromotek) or RFP-trap beads (Chromotek) for mCherry-GATAD2B. Incubation and wash buffers are as described before (Baymaz et al., 2014); incubation in Buffer C (300 mm NaCl, 20 mm Hepes/KOH, pH 7.9, 20% v/v glycerol, 2 mm $MgCl_2$, 0.2 mm EDTA, complete protease inhibitors) with 0.25% NP40 and 50 ug/mL ethidium bromide. After one hour incubation, 6 washes were performed: 2 with Buffer C and 0.5% NP-40, 2 with PBS and 0.5% NP-40, and 2 with PBS. On-bead digestion was performed using Trypsin (Baymaz et al., 2014), followed by desalting of the peptides on StageTips (Rappsilber et al., 2003).

Mass spectrometry

Tryptic peptides were separated using an EASY-nLC1000 (Thermo) HPLC connected to either an LTQ-Orbitrap Velos, LTQ-Orbitrap QExactive or an Orbitrap Fusion Tribrid (Thermo Fisher Scientific) mass spectrometer. Peptides were eluted from the HPLC column using a ~2-hour acetonitrile gradient.

Raw data were analyzed using MaxQuant software package 1.5.1.0. Default settings were used, except for the following options:

For SILAC experiments we used multiplicity 2 for SILAC experiments, and checked the "re-quantify" box (Cox and Mann, 2008). We filtered for contaminants and reverse hits using Perseus. 1.2.7.4. The normalized forward and reverse ratios were logarithmized and significance B was calculated, after which two-dimensional scatterplots were made using R.

For label-free based quantification (LFQ) (Cox et al., 2014), MaxQuant was applied using multiplicity 1 and boxes for 'match between runs' and 'iBAQ quantification' checked. We filtered for contaminants and reverse hits using Perseus 1.2.7.4. The LFQ intensities were logarithmized and triplicates were assigned to the same group. We then filtered for 3 valid values in at least one group, assuming that specific interactors may only be identified in the triplicates of that specific purification. Missing values were imputed using a normal distribution and default settings. A two-sample adapted *t*-test was performed between the control and the experiment in Persues to obtain p-values for each protein, after which volcano plots were made using R. Stoichiometry determination was performed as described in Smits et al. for the significant proteins (Smits et al., 2013). Basically, the mean iBAQ intensity of a protein in the control purifications is subtracted from each of the experimental purifications. Then, the remaining values are divided by those of a protein that is monomeric in the complex. The average of these relative abundances is then plotted in a bar graph. For proteins that share peptides, the iBAQ intensities are summed before the stoichiometry calculation.

For calculation of relative abundance of proteins that share many peptides, a different approach was used. Normalized unique intensities are calculated by using the sum of the intensities of unique peptides in each sample in the stoichiometry calculation instead of the iBAQ value. Note that this calculation only gives information about a single protein in the different conditions, since the values are not normalized for protein size.

The mass spectrometry data have been deposited to the ProteomeXchange Consortium via the PRIDE (Vizcaino et al., 2016) partner repository with the dataset identifier PXD003856. Analyzed mass spec data can be found in Table S1 according to the following scheme:

Tab	Experiment	Method	Figure(s)	Raw file date
1	MBD3-GFP	SILAC	1A	20130227
2	GFP-ZMYND8^{WT}	SILAC	1B	20140515
3	MBD2-GFP	SILAC	S1A	20140221
4	MBD3-GFP shSCR, shCDK2AP1, shZMYND8, shZNF687	LFQ	1C	20131223
5	GFP-GATAD2A in Control and ZMYND8-KO cells (clone #21) GFP-GATAD2B in WT cells	LFQ	1F,G, S1H 2A,B,C,S2A,B	20160504/20151112 20151112
6	GFP-ZMYND8 mutants	LFQ	1D,S1D,E,F	20130916
7	GFP-ZMYND8^{MYND}	SILAC	1E	20131119
8	GFP-ZMYND8$^{\Delta MYND}$	SILAC	S1G	20130628
9	MBD2-GFP in shSCR/GATAD2A/B cells	LFQ	2D,S2D	20160719
10	GFP-GATAD2A^{WT}	SILAC	S2G	20140508/20140515
11	GATAD2A$^{\Delta PPPL\Phi}$	SILAC	S2G	20150421 (deletion not in raw-file name)
12	GATAD2A^{PPPLP}	SILAC	S2G	20150529
13	MBD3-GFP/GFP-ZMYND8 w/ or w/o phleomycin	LFQ	S4C,D	20160628 (start date)

Bacterial expression
GST and GST-MYND proteins were expressed in CD600 bacteria. Bacterial cultures were grown at 37°C until OD600 was 0.6. Then expression was induced using IPTG and cultures were grown at 25°C for three hours. Bacterial pellet was lysed in the following buffer: 50 mM Tris-HCl pH 8.0/ 20% sucrose/ 1 mM EDTA/ 0.5 mM PMSF/ 1 mM DTT/ 1 µg/ml aprotinin, 0.1% Triton-x100, and 0.1 mg/ml lysozyme. Bacterial debris was removed by ultracentrifugation.

GST-pull downs
Bacterial lysate containing GST (30µl) or GST-MYND (120µl) was incubated with 45 µl glutathione beads for one hour in a total volume of 250 µl in bacterial lysis buffer (50 mM Tris-HCl pH 8.0/ 20% sucrose/ 1 mM EDTA/ 0.5 mM PMSF/ 1 mM DTT/ 1 µg/ml aprotinin with 0.05% NP40). Beads were then washed: 2x incubation buffer, 2x Buffer C300 (same as GFP affinity purification). Next, 0.5 mg of nuclear extract containing GFP, GFP-CR1 or GFP-PPPLΦ in a total volume of 400 µl in buffer C300 with 0.25% NP40 was incubated with the beads in the presence of EtBr (50 µgr/ml final concentration) for 2 hours. Beads were washed 4x using buffer C300-0.25% NP40 and resuspended in SDS sample buffer.

ChIP-sequencing
Sub-confluent Hela Kyoto cells were fixed using DSG for 45 minutes, followed by formaldehyde crosslinking for 10 minutes. Cells were collected and sonication was used to shear the chromatin into 100-300 bp fragments using a Biorad picoruptor. Antibodies (see list of used antibodies) were incubated with chromatin overnight. Prot A/G dynabeads (Thermo Fisher Scientific) were added and incubated for 1.5 hours. After extensive washing,DNA was de-crosslinked for 4 hours at 65^{o}C in the presence of Prot K. DNA was purified using the Qiagen MinElute kit. Library prep was performed using the KAPA kit and Nextflex adaptors. After this, purified DNA was analyzed by deep sequencing on the Illumina GAIIx or Illumina HiSeq2000 genome analyzers. For qPCR analysis, samples were used after the minElute purification. A list of ZMYND8 target genes can be found in Table S2.

Antibodies

Antibody	Host	Company (reference)	IF	WB	ChIP
CHD4	Rabbit	Active Motif (39289)	1:500		3 µl
GATAD2A	Rabbit	Bethyl (A301-282A)	1:500	1:1000	3 µl
GATAD2B	Rabbit	Bethyl (A301-282A)		1:1000	
MDC1	Rabbit	Abcam (ab11171-50)	1:1000		
PAR (10H)	Mouse	Abcam (ab14459)	1:100		
RAD51	Mouse	GeneTex (clone 14B4)	1:100		
Tubulin	Mouse	Sigma (T6199)		1:5000	
ZMYND8	Rabbit	Sigma (HPA020949)	1:100	1:1000	3 µl
GFP	Rabbit	Abcam (ab290)		1:3000	3 µl
Histone H3	Rabbit	Abcam (ab1790)			3 µl
MBD3	Rabbit	Bethyl (A302-528A		1:1000	3 µl
MBD3	Mouse	IBL (3A3)		1:3000	
MBD2	Goat	Everest Biotechnology (EB7538)		1:3000	
GST	Rabbit	Santa Cruz (B-14, sc-138)		1:2000	
γH2AX	Mouse	Millipore (clone JBW301)	1:2000		
α-Rabbit Alexa488	Goat	ThermoFisher (A11034)	1:1000		
α-Mouse Alexa488	Goat	ThermoFisher (A11029)	1:1000		
α-Rabbit Alexa555	Goat	ThermoFisher (A21429)	1:1000		
α-Mouse Alexa555	Goat	ThermoFisher (A21424)	1:1000		
α-Rabbit Alexa647	Goat	ThermoFisher (A21245)	1:1000		
α-Mouse Alexa647	Goat	ThermoFisher (A21235)	1:1000		

Library sequencing and data analysis

The 36 (GAIIx) or 43 bp (HiSeq2000) tags were mapped to the reference human genome hg19 (NCBI build 37), using BWA allowing one mismatch. PCR duplicates were removed and the number of reads was randomly downsampled to match the reference input sample.Peak-calling was performed with the MACS 2.0 toolZMYND8 peaks and their assigned target genes are listed in Table S2. All high-throughput sequencing data is available as GSE79836. (http://www.ncbi.nlm.nih.gov/geo/query/acc.cgi?acc=GSE79836)

The Python package used for K-means clustering and generation of Heatmaps and bandplotsis available at http://simonvh.github.io/fluff/ (Georgiou and Van Heeringen, 2016). R was used to generate bandplots.

Available RCOR1 ChIP-seq data in HeLa S3 (GSM1104353**)** was used for heatmaps**.** DNA methylation was analyzed using GSM999337. The intersection between all promoters (TSS+/-1kb) and the DNA methylation of the 450K probes was used to select the hyper-methylated (>0.8) and hypo-methylated (<0.4) promoters. The same was done for ZMYND8 bound loci, per cluster, and for all active enhancers. These files were then used to make bandplots. The ChIP-Seq datasets for H3K4me1, H3k27ac, DnaseI and P300 were retrieved from the ENCODE data repository site (http://genome.ucsc.edu/ENCODE/).

RNA-seq

Hela FRT-TO CRISPR cell lines were seeded in 6-well dishes with dox-induction for 48 hours. Cells were harvested and RNA was purified using the Qiagen RNeasy kit. Ribosomal RNA was removed using the RiboZero kit (Illumina). RNA was then fragmented in fragmentation buffer (40 mM Tris-acetate, 100 mM Potassium Acetate, 30 mM Magnesium Acetate, pH 8.2). The first cDNA strand was synthesized with Reverse Superscript III in the presence of Actinomycin D and random hexamers. Second strand was synthesized with E.coli DNA polymerase in the presence of dUTP. The library preparation was as described for ChIP-seq, with the exception that USER enzyme was added prior to library amplification to maintain strand identity.

The 42-bp paired-end reads were aligned to hg19 using the Genomic Short-read Allignment Program (Wu and Watanabe, 2005), allowing for one mismatch. Aligned reads were sorted and indexed with the BamTools API 1.0.2 (Barnett et al., 2011). Differential transcript expression analysis was performed using the cuffdiff tool in the Cufflinks v2.1.1 package (Trapnell et al., 2010), by quantifying Fragments Per Kilobase of transcript per Million reads mapped on the human RefSeq transcript database (Pruitt et al., 2014) downloaded on 18-01-2016.

UV-A laser micro-irradiation

Cells were grown on 18 mm coverslips and sensitized with 10 µM 5′-bromo-2-deoxyuridine (BrdU) for 24 hrs. When required, cells were simultaneously induced with 2 µg/ml doxycycline. For micro-irradiation, the cells were placed in a Chamlide TC-A live-cell imaging chamber that was mounted on the stage of a Leica DM IRBE widefield microscope stand (Leica) integrated with a pulsed nitrogen laser (Micropoint Ablation Laser System; Andor). The pulsed nitrogen laser (16 Hz, 364 nm) was directly coupled to the epifluorescence path of the microscope and focused through a Leica 40x HCX PLAN APO 1.25-0.75 oil-immersion objective. The growth medium was replaced by CO_2-independent Leibovitz's L15 medium supplemented with 10% FCS and penicillin-streptomycin and cells were kept at 37°C. The laser output power was set to 72 to generate strictly localized sub-nuclear DNA damage. Typically, an average of 50 cells was micro-irradiated (2 iterations per pixel) within 5 min using Andor IQ software (Andor).

Immunofluorescent labelling and image acquisition

Five minutes after micro-irradiation, cells were pre-extracted with 0.25% Triton-X100 (Serva) in cytoskeletal (CSK) buffer (10 mM Hepes-KOH, 300 mM Sucrose, 100 mM NaCl, 3 mM $MgCl_2$, pH 7.4) for 2 min and subsequently fixed with 4% formaldehyde in PBS for 20 min at room temperature. Cells were post-extracted with 0.5% Triton-X100 (Serva) in PBS for 5 min, and treated with 100 mM glycine in PBS for 10 min to block unreacted aldehyde groups. Cells were rinsed with PBS and equilibrated in WB (PBS containing 0.5% BSA, and 0.05% Tween 20; Sigma-Aldrich) for 10 min. Antibody steps and washes were in WB.

Primary antibodies were incubated overnight at 4°C. Detection was done using goat anti-mouse Ig coupled to Alexa 555 and goat anti-rabbit Ig coupled to Alexa 488 or 647 (1:1000; Invitrogen Molecular probes). Samples were incubated with 0.1 µg/ml DAPI and mounted in Polymount. Images of fixed samples were acquired on a Zeiss AxioImager M2 widefield fluorescence microscope using a 63x PLAN APO (1.4 NA) oil-immersion objective (Zeiss) and an HXP 120 metal-halide lamp used for excitation. Images were recorded using ZEN 2012 software and quantified using Image J.

HR assay

U2OS cells containing a stably integrated copy of the DR-GFP reporter were used to measure the repair of I-SceI-induced DSBs by HR as described (Pierce et al., 1999). Briefly, 48 hrs after siRNA transfection, the cells were co-transfected with an mCherry expression vector and the I-SceI expression vector pCBASce. After again 48 hrs the percentage of GFP-positive cells among mCherry-positive cells was determined by FACS on a BD LSRII flow cytometer (BD Bioscience) using FACSDiva software version 5.0.3.

Cell cycle profiling

For cell cycle analysis, cells were fixed in 70% ethanol, followed by DNA staining with 50 µg/ml propidium iodide in the presence of RNase A (0.1 mg/ml) (Sigma). Cell sorting was performed on a LSRII flow cytometer (BD Bioscience) using FACSDiva software (version 5.0.3; BD). Quantifications were performed using Flowing Software.

(RT-)qPCR

Real-time quantitative PCR was applied to test expression levels of genes. Shortly, RNA was purified using the RNeasy kit (Qiagen). cDNA was prepared using iSCRIPT reverse transcriptase (BioRad). Detection of cDNA was performed using iQ Sybr green mix (BioRad) on a CFX96 RT-PCR machine (BioRad). A dilution series of a cDNA pool was used to obtain expressin values, that were then normalized for β-ACTIN in the same sample.

RT-qPCR Primers	
TXLNA_F	GACCAAATCAACCAATCACTACAGC
TXLNA_R	ACACTGGCCTTCACTCATGGATA
CEP1_F	CACTGTATGTCCAAGCAAGCAGA
CEP1_R	GTGACCAATTCCCCTAAAGCATC
GATAD2A_F	CTCTTTGGGTGTGGAGGCTGT
GATAD2A_R	CATCTGGTGGCAAACATTTCTT
GATAD2B_F	GAGGGGAACAAGACCCTTTTG
GATAD2B_R	ATCTGTCACTGCTGAAATGCTCA
B-actin_F	AGAAAATCTGGCACCACACC
B-actin_R	AGAGGCGTACAGGGATAGCA

For ChIP-qPCR, purified DNA after the ChIP was quantified using loci-specific primers. A dilution curve was made starting with 5% input chromatin, which was used to calculate enriched DNA. Primers are shown in the below table.

ChIP-qPCR primers	
NDRG1_F	GCTGCTCTGTTTGTGCGTAACTA
NDRG1_ R	GGCTCCTCTGGGACTTCTCATAT
HPD _F	GGTGGGGATTAAAGGAGATAAGCA
HPD _R	GGAATGTTCTCTGTCCCAATGAA
NOTCH2NL_F	AGGAGAAGTAGGGCAACTGGTGT
NOTCH2NL_R	CGCGCCTCAGAAAGAATAACAG
LBH _F	TGGGTCACTCCTTATGCTACCAA
LBH _R	AACCTGTCATTCCTTGCTGTCTG
ADAM15_F	TTAGTGACAGCAACGACGACACT
ADAM15_R	GTGAAGCGTACAGGGCATTTTAT
MYOD1_chpF1	CGCCAGGATATGGAGCTACTGT
MYOD1_chpR1	GAAACACGGGTCGTCATAGAAGT

Supplemental References

Ran, F.A., Hsu, P.D., Wright, J., Agarwala, V., Scott, D.A., and Zhang, F. (2013). Genome engineering using the CRISPR-Cas9 system. Nat Protoc *8*, 2281-2308.

Rappsilber, J., Ishihama, Y., and Mann, M. (2003). Stop and go extraction tips for matrix-assisted laser desorption/ionization, nanoelectrospray, and LC/MS sample pretreatment in proteomics. Anal Chem *75*, 663-670.